Study of the LHCb Muon Detector performance using 2010 beam data

LHCb Public Note

Issue: 1
Revision: 0

Reference: LHCb-PUB-2011-027
Created: January 5, 2011
Last modified: December 21, 2011

Prepared by: Giacomo Graziani [a], Roberta Santacesaria [b], Alessia Satta [c]
[a]INFN sezione di Firenze
[b]INFN sezione di Roma
[c]INFN sezione di Roma Tor Vergata

LHCb-PUB-2011-027
21/12/2012

Abstract

The performance of the LHCb muon detector chambers is evaluated in terms of operability, noise, cross–talk, time resolution and efficiency using data collected during the 3.5 TeV p-p collisions run of the LHC in 2010.

Contents

1 Introduction

The LHCb muon detector is used online in level–0 (L0) and high–level (HLT) triggers and for the offline muon identification. All these applications require a very high efficiency in the very short LHC time gate. The most stringent requirement is dictated by the L0 trigger, which, in order to effectively reduce the background, asks the muon system to give a signal in all the five stations. To efficiently satisfy such requirement the muon chambers were designed to have a detection efficiency larger than 99% within the 25 ns LHC gate [1].

Cosmic data and collision data acquired in 2009 were used for the first calibrations with physics signals and the the first evaluation of performance [2], but the precision was limited by statistical and systematic uncertainties .

The large p-p collisions data sample made available by the 2010 LHC run allowed for improving these results, and in particular for a precise determination of the chamber efficiency.

In this note, after summarizing the main features of detector operations during 2010, we first evaluate the average response to muon tracks in terms of cluster size, to evaluate the cross–talk among adjacent detector channels. Particle rates are measured, verifying their scaling with luminosity over the wide range of beam intensity spanned during the 2010 data taking. We then describe the improvements on timing calibration and the resulting time resolution. Finally, an accurate measurement of the chamber efficiency is presented. After discussing the method for background subtraction and a check of the procedure, results are reported, including an estimate of the systematic uncertainties.

2 Detector Operability

2.1 Detector Settings

The operating conditions, thresholds and high voltages, of the muon detector for the 2010 run have been optimized through a procedure that is described elsewhere[3, 4], aimed at reaching low and stable noise rate (thresholds were set to 6 noise r.m.s.), while minimizing ageing effects and cross–talk by chosing the minimal high voltage value in each region allowing to obtain the required 99% efficiency. The resulting HV values for the different types of MWPC are listed on table1.

Table 1 High Voltage settings, in kV, for the MWPCs of different detector regions.

	R1	R2	R3	R4
M1		2.60	2.62	2.58
M2	2.53	2.61	2.59	2.56
M3	2.53	2.62	2.59	2.57
M4	2.57	2.63	2.64	2.58
M5	2.58	2.64	2.65	2.60

These settings were kept constant during the whole 2010 run, except for region M5R2 for which voltage was reduced from 2.64 to 2.55 kV on august 12th in order to reduce the rate of HV trips. Thresholds were lowered correspondingly to mantain high efficiency at the price of a slight increase of the noise level.

The triple GEM detectors of M1R1 were operated with voltages of 435/425/415 V for the first part of the run. Voltages were reduced twice by 5 V per gap for safer operations following the increasing luminosity, on july 12th and october 14th.

2.2 Detector Operations in 2010

Figure 1 shows the typical map of muon hits in all five stations during a physics run. The few holes that are marked on the maps correspond to the hardware problems listed on table 2. Most of the dead channels are due to hardware problems in the readout chain and were known since the beginning of the data taking. The majority are on the M1 station because of its late commissioning. They affect only 129 of the 55296 logical pads (0.2%). The effect on muon tracking efficiency is estimated by counting the fraction of muon tracks with momentum larger than 6 GeV crossing one of the dead channels in MonteCarlo minimum-bias events. It is found to be below 1 %.

Detector failures that occurred during the run are mostly due to HV trips of some detector gap. Damages were permanent (shorts inside the chambers) for 10 (7 MWPC and 3 GEMs) of the 4968 gaps (0.2%); in all other cases gaps were recovered after some conditioning procedure.
For M2–M5 stations, due to the large redundancy (4 independent gaps per chamber), effects on the overall system efficiency are expected to be negligible (< 0.1 %).
In the case of M1, trips are potentially more dangerous since there are only 2 gaps per chamber. However, this station is only used by the L0 trigger and not by the high level trigger and offline reconstruction. If detectors in a whole trigger sector are faulty, the corresponding link to the L0muon trigger can be forced to one for all events. In this way, the effect is limited to a slight degradation of the L0muon performance for the affected region. This procedure was needed only in one case, chamber A16A2 in M1R1, when both its triple GEM detectors became very inefficient on oct 14th.

Noise in the detector should be below 1 kHz (per physical channel) in order to have a negligible rate (below 1 Hz) of fake muon candidates in the muon trigger. Even lower rates are desirable to suppress the noise contribution to muon misidentification in the offline reconstruction.

The level of detector noise was checked regularly with some dedicated runs with random triggers in the absence of beam. From the multiplicity of firing logical channels (for double readout regions) or logical pads, the rate of noise per physical channel is computed for each detector region. The typical result is shown on fig. 2 for two runs acquired on june 2nd and october 23th, 2010. For most channels, noise is below 10 Hz. Only region M5R2, after the mentioned decrease of high voltage and thresholds, was operated with an average noise per physical channel of about 100 Hz. The fraction of channels having noise larger than 10 kHz is typically lower than 0.1%. The rate of L0muon candidates due to noise was always negligible ($\ll 1$ Hz).

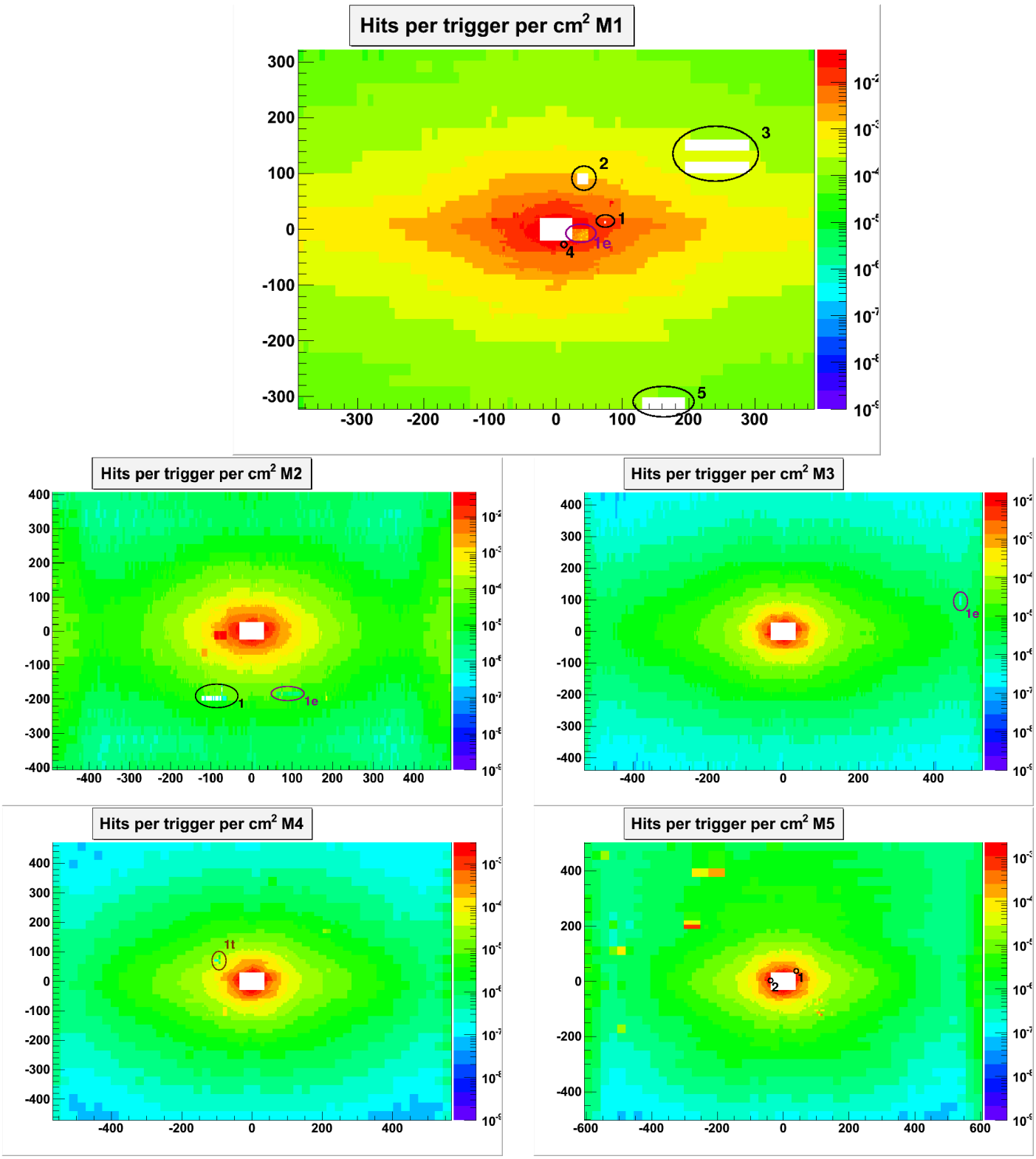

Figure 1 Illumination map of the five detector stations in a typical 2010 physics run. The plots show the number of hits per cm^2 on log scale for all the 55296 logical pads. Faulty channels giving no hits are marked and listed on table 2. A few noisy spots can be noticed as well.

Table 2 List of dead channels of the muon detector, covering the whole 2010 data taking.

ID	Logical Channel	#log. ch.	#log. pads	Chamber/FEB	Comments	estimated effect on muon tracking efficiency (%)
M1-1	Q1M1R2_1/68	1	1	M1A17A3	dead since april 5, 2010	0.04
M1-2	Q1M1R3_3/16-23	8	8	M1A21A	sync masked for hardware problem	0.07
M1-3	Q1M1R4_1/108-119 156-167	24	24	M1A22C/A24C	2 chambers with gas problems	0.2
M1-4	Q2M1R1_3/191	1	1	M1A15A1	masked at sync level (noisy)	0.003
M1-5	Q2M1R4_3/184-191	8	8	M1A1B FEBS1-2	2 FEBS with LV problems	0.01
M1-1e				A16A2	GEM very inefficient since oct 14.	0 (3.0 if L0muon was not forced)
M2-1	Q3M2R3_2/36,62	2	27	M2C9A,C10A	2 dead SYNC channels since oct 4, 2010	0.02
M2-1e	Q2M2R3_2/37,61	2	27	A9A, A10A	inefficient sync channels since oct 4, 2010	0.01
M3-1t	Q2M3R2_1/2,18	2	24	A16A3	inefficient channels, unstable timing	0.4
M3-1e	Q1M3R4_1/174x190	0	1	A20D	inefficient FEB channel	0.0007
M4-1t	Q4M4R2_1/99,106	2	6	M4C19A3	inefficient channels, unstable timing	0.06
M5-1	Q1M5R1_1/104	1	1	M5A18A2	masked at sync level (noisy)	0.006
M5-2	Q4M5R1_1/0	1	1	M5C17A2 FEB 0	dead sync channel?	0.006
TOTALS		52	129			0.8%

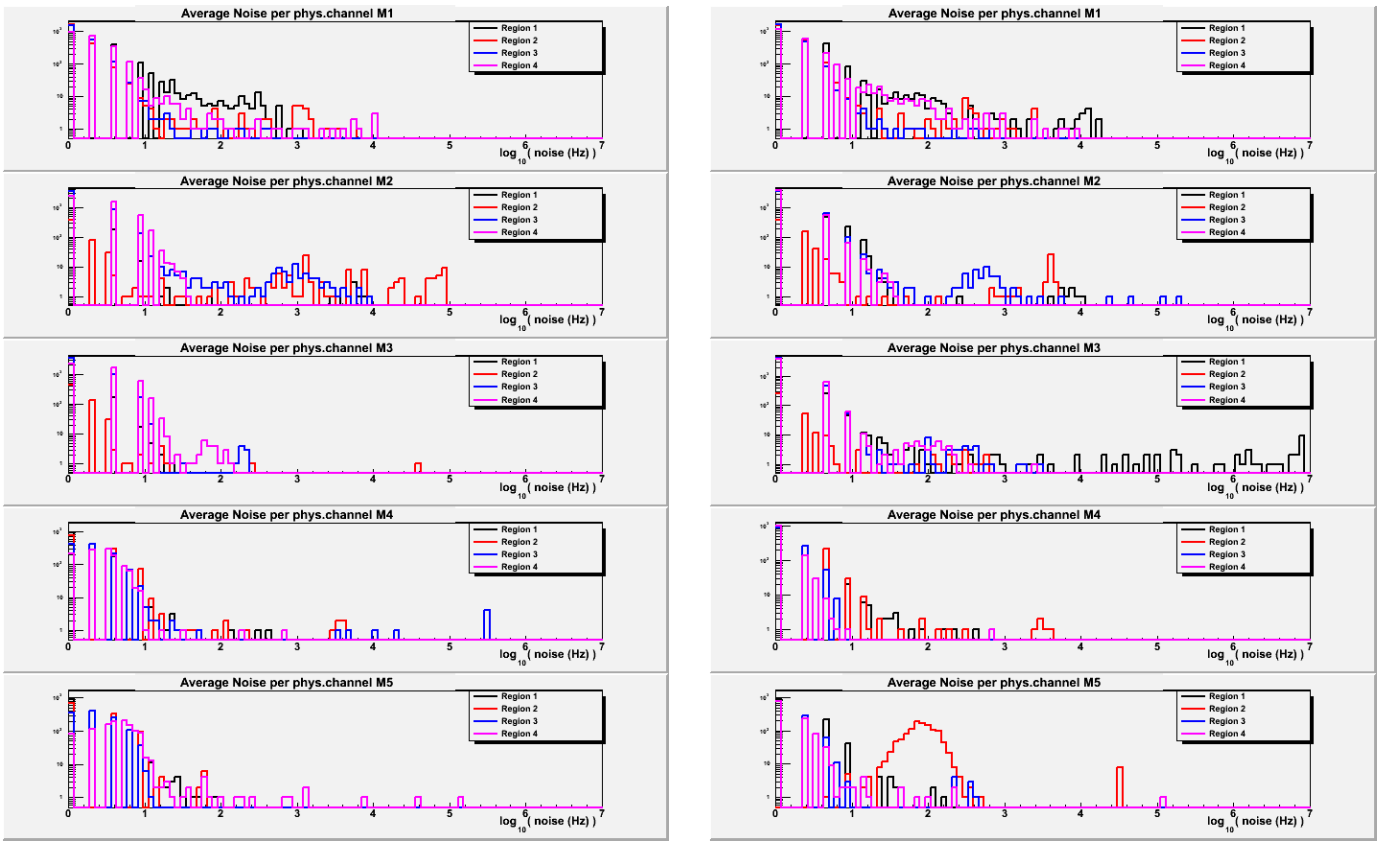

Figure 2 Distribution of noise rate per physical channels for all detector regions. The left plot refers to run 72743 (june 2nd), the right plot to run 81267 (october 23th). The first bin contains all channels with noise lower than 10 Hz. The change in the noise figure for region M5R2, after the threshold lowering, can be noticed.

3 Data samples and track reconstruction

The data consist of p-p collisions at $\sqrt{s}$=7 TeV taken during the 2010 LHC run. Due to the continous progress of the LHC machine operations, these data span a wide range of luminosity values, from 10^{27} to 10^{32} Hz/cm^2. The filling scheme was accordingly evolving with time, from the single bunch collision per orbit of the first runs, to the 150 ns spaced bunch trains of the highest intensity runs with 344 collisions per orbit (equivalent to a 3.9 MHz collision rate) and the first tests with 50 ns spaced bunches.

In order to test the muon detector response with these changing conditions, a set of sample runs, listed in table 3, was chosen. These include some special runs acquired with a larger time gate (125 ns instead of the nominal 25) for time alignment studies (TAE events in the following).

For the measurement of particle rate, cluster size and time resolution we used only events triggered by some minimum bias condition independent of the muon detector response:

- L0 Minimum Bias (L0MB in the following), requiring the total energy released in the HCAL to be more than 320 MeV;
- "Microbias" single track trigger (μbias in the following), requiring some hits compatible with a track in the VELO or first Tracking stations;
- random triggers.

We evaluate for each sample run the average number of interactions visible in the LHCb detector per beam crossing μ from the fraction f_0 of beam crossing events not producing a μbias trigger

$$f_0 = P(0;\mu) = e^{-\mu} \tag{1}$$

where P is the Poisson distribution.

Table 3 List of sample LHCb 2010 runs used for checking the detector response as a function of luminosity. The average number of visible interactions per beam crossing μ and the pile–up factor $p = \mu/(1 - f_0)$, giving the average number of visible interactions for visible events, are also reported.

Run N.	Luminosity (Hz/cm^2)	μ	p	bunch crossings per orbit	Notes
70276	1.3 $\times 10^{27}$	0.008	1.004	1	
70493	2. $\times 10^{27}$	0.012	1.006	1	TAE events
70686	5. $\times 10^{27}$	0.016	1.008	2	
72331	8. $\times 10^{28}$	0.062	1.031	8	
75411	1. $\times 10^{30}$	0.754	1.424	8	
78329	6. $\times 10^{30}$	1.021	1.596	36	
79884	2. $\times 10^{31}$	1.489	1.923	93	150 ns trains
79949	4. $\times 10^{31}$	1.782	2.142	140	150 ns trains
80396	7. $\times 10^{31}$	1.815	2.168	233	150 ns trains
81350	1.5 $\times 10^{32}$	2.622	2.827	344	150 ns trains
81811	1.6 $\times 10^{31}$	1.042	1.610	90	50 ns trains

However, the statistics of muon tracks in the minimum bias samples was not adequate for the measurement of the efficiency, for which the events acquired with the standard physics triggers were used as described in the following.

For the efficiency of M2-M5 stations, we used the data acquired during the machine fills 1122 and 1134 (may-june 2010, runs 72325 – 72909). They correspond to an integrated luminosity of 0.8 and 0.6 nb^{-1} respectively. The trigger required a high p_T hadron or lepton detected in the calorimeter or in the muon system at the first, hardware, level (L0); due to the low luminosity only the first part of the software high–level trigger (HLT1) was executed and the decision was the OR of several independent algorithms (TCK 0x00091710). Since the muon information is an important ingredient of the trigger decisions, we had to remove the bias introduced by the trigger in the efficiency calculation. This is done by selecting events where both L0 and Hlt1 were fired irrespectively of the muon system information. With this selection the majority of the muons reaching the muon stations and used for this analysis originate from decay in flight of π's or K's.

For the M1 efficiency measurement, kaons decaying between the tracking stations and M1 station would deteriorate the quality on the prediction which is essential because the occupancy is much larger here than on M2-M5 stations. To have a sample of true muons, events with a reconstructed $J/\psi \rightarrow \mu^+\mu^-$ were used. This sample corresponds to almost all data acquired in 2010 (about 37 pb^{-1}). In the trigger algorithms the M1 information is used only for L0. The high level trigger, the reconstruction and the data stripping do not use it. To remove the L0 bias on the efficiency evaluation, in each μ^+ μ^- couple from a J/ψ, the muon which fired the L0 trigger was not considered in the analysis. Notice that the use of the J/ψ sample for the analysis of M2-M5 station is not possible since the muon information is used to identify both muons in the HLT and in the reconstruction.

MonteCarlo samples were also used to compare the observed and expected detector performance, and to verify the analysis procedures. We used some of the standard samples produced by the LHCb collaboration simulating minimum bias p-p interactions and collisions with a prompt J/ψ decaying to $\mu^+\mu^-$. Some special samples used for particular needs will be described on the next sections. The events were generated using PYTHIA 6.4 [11] to describe the p-p collisions and GEANT4 [12] for the LHCb detector simulation.

The muon track reconstruction algorithm used in this note is a standalone algorithm similar to the one used in the muon high level trigger [10]. Tracks are reconstructed starting from the firing logical pads. Pads with common sides are clusterized to obtain track hits, whose spatial coordinates are obtained from the barycenter of the pad central positions. Aligned hits in the muon stations with the primary proton-proton collision point are selected by a combinatorial algorithm. The track hits are fitted to a straight line and quality cuts are applied depending on the measured quantities. These standalone tracks are then matched with the tracking detectors when this is needed to improve momentum resolution or reduce background.

4 Cross Talk

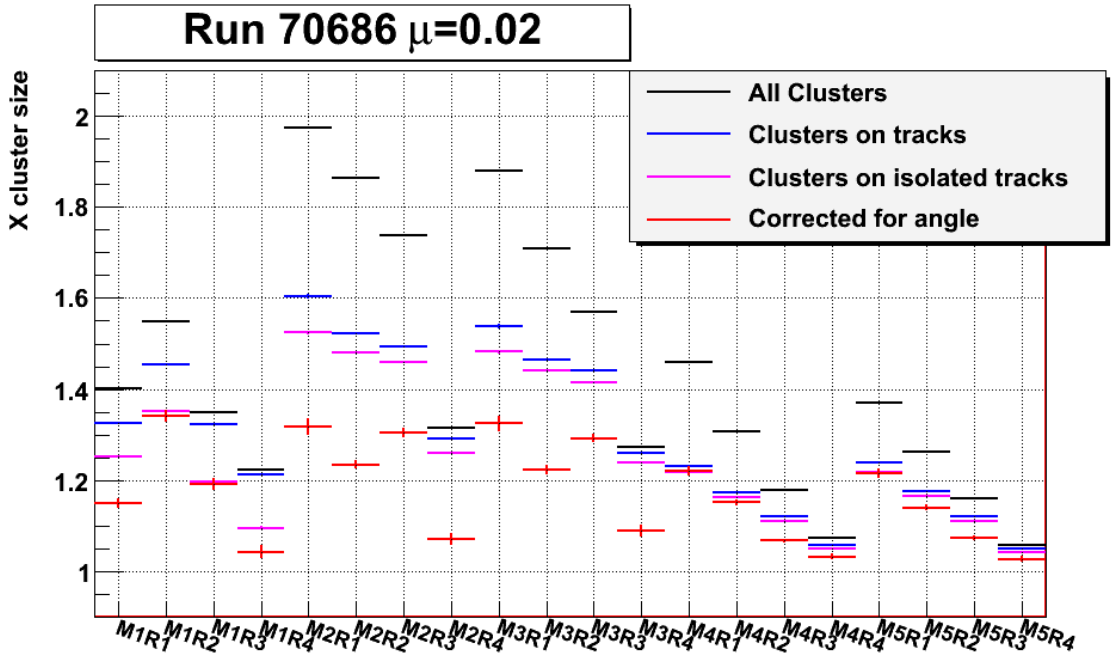

Figure 3 Average cluster size along the x direction in each detector region. Events are triggered by μbias or L0MB triggers, and the different selections described in the text are compared.

The average cluster size of muon hits is an essential parameter of the detector response, since it monitors the correct operation conditions of the chambers and affects the muon trigger performance. It can be measured in terms of average number of firing adjacent muon pads. Due to the finer segmentation of chambers in the x (bending) direction, cross–talk mostly happens among adjacent pads in x and is expected to induce an average cluster size larger than 1, depending on the gain over threshold settings and detector geometry of each region. A significant cross–talk among adjacent pads in the y (vertical) direction is observed only in regions with double readout (stations 2 and 3 in regions 1 and 2) where cathode pads are designed to provide the y coordinate. In the following, we will study the cross–talk considering the cluster size in the x direction.
The expected values for the nominal operating conditions were carefully measured on test benchs and used to feed the MonteCarlo simulations.

For the most illuminated regions, a large contribution to the average size of clusters seen in the detector can be ascribed to punch–through showers and backscattered particles. The cluster size is indeed smaller for clusters associated to reconstructed muon tracks, as shown on figure 3. If track clusters are also required to be isolated, asking for no adjacent firing pads in the non bending direction (y cluster size =1) and no other firing channels in the same station within 7 logical pads in the x (bending) direction and 2 logical pads in y, the cluster size gets also significantly smaller, demonstrating a clear pile–up effect that is dependent on the run conditions. This can also be verified in figures 4 and 5, where we compare the cluster sizes for different values of the average number of visible interaction per beam crossing μ. The MC data in the 2010 configuration exhibit a smaller pile–up effect compared to real data at similar μ, due to the lower detector rates predicted for M1 and inner regions, as will be discussed in more detail on section 5. The isolation cut reduces the effect of pile–up though not fully suppressing it.

Finally, the purely geometrical effect due to the track trajectory inside chambers can be measured by plotting the average x cluster size as a a function of the angle between the track projection on the bending plane and the direction perpendicular to the chamber surface. We correct the effect by extrapolating to 0 angle, as shown in fig. 6.

The resulting average cluster size after all corrections quantifies the amount of cross–talk in each region. Values are compared with the expectations from the MC data in figure 7. They are in good agreement with the design performance used in the simulation, and even slightly better for most regions thanks to the careful optimization

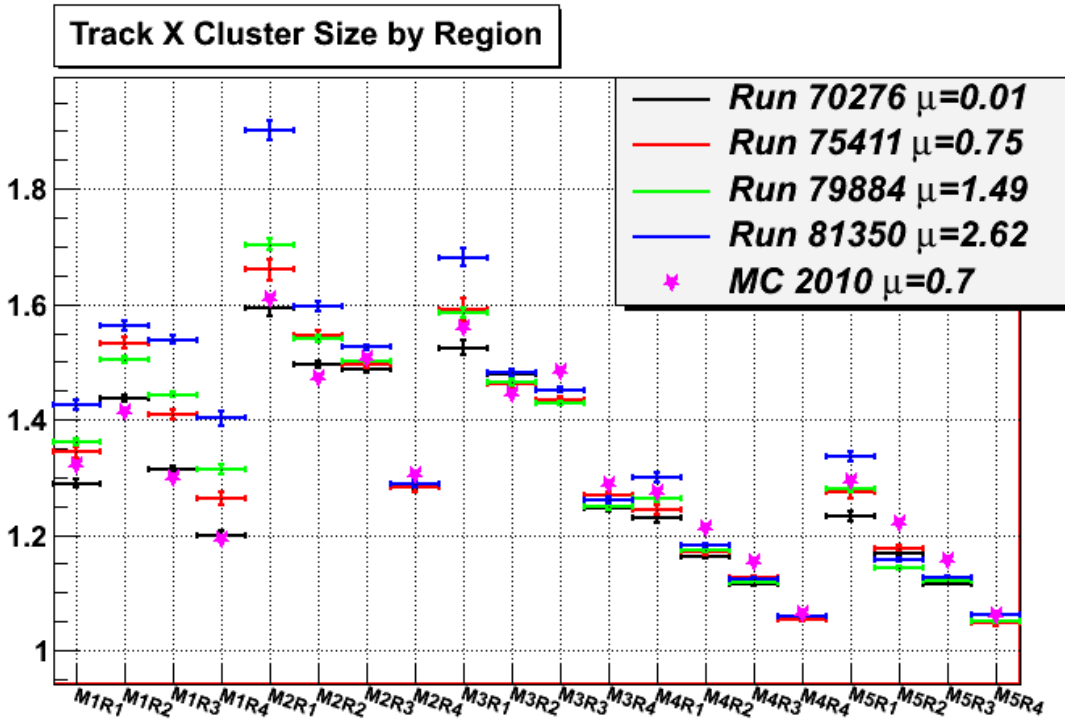

Figure 4 The average cluster size for all track hits in each region is shown for different μ values. A clear pile–up effect can be observed for the most illuminated regions. MC2010 data, produced with $\mu = 0.7$, are also shown for comparison.

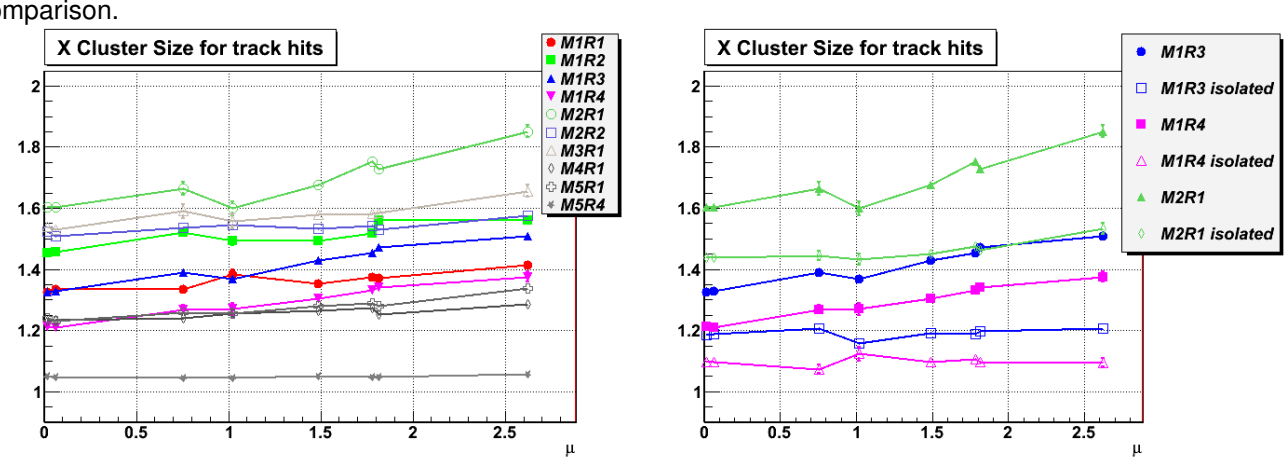

Figure 5 The average cluster size for track hits is plotted on the left as a function of μ for some sample regions. On the right plot, the effect of the isolation cut in reducing the μ dependence can be observed.

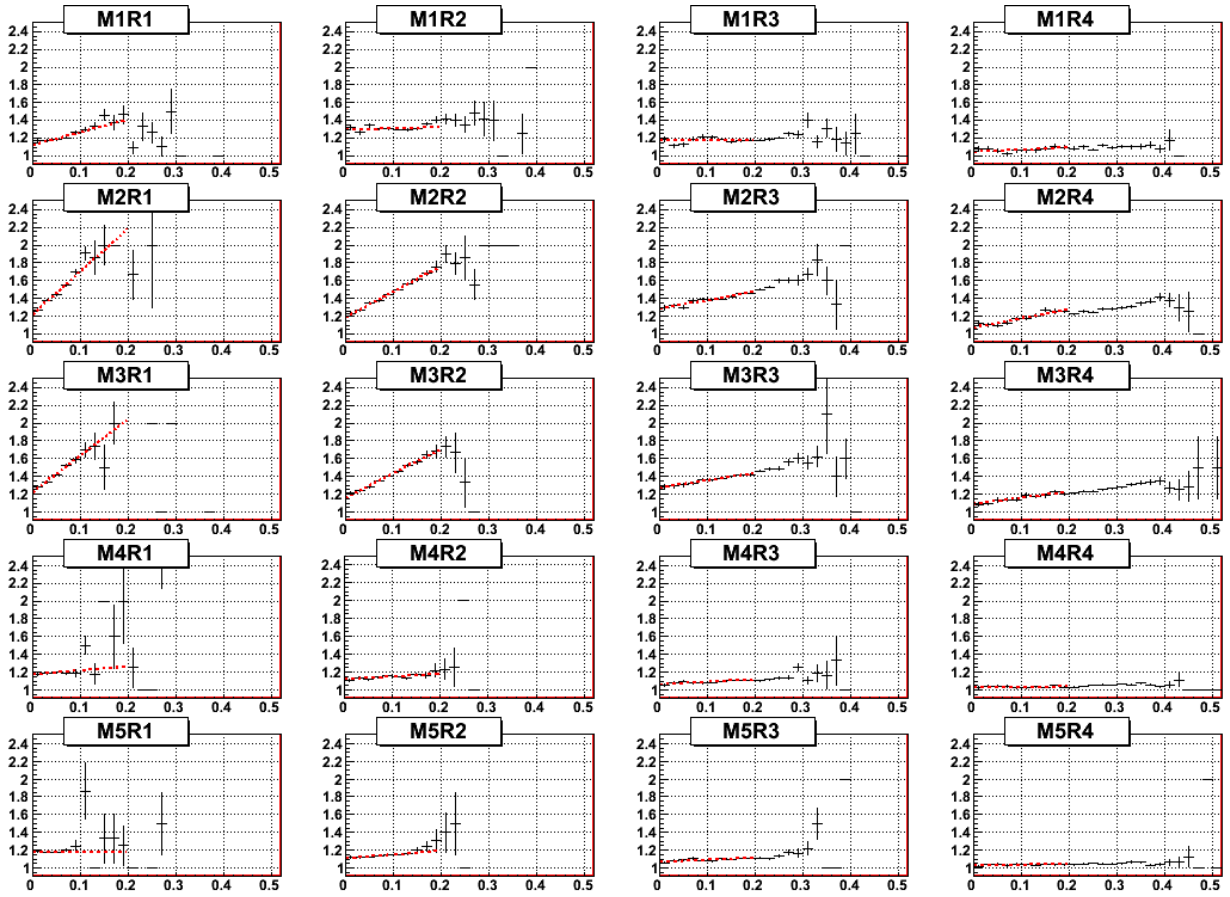

Figure 6 Average x cluster size for isolated track hits as a function of the track angle (in rad). A linear extrapolation is used to correct for the geometrical effect and extract the average cluster size due to cross talk in each region.

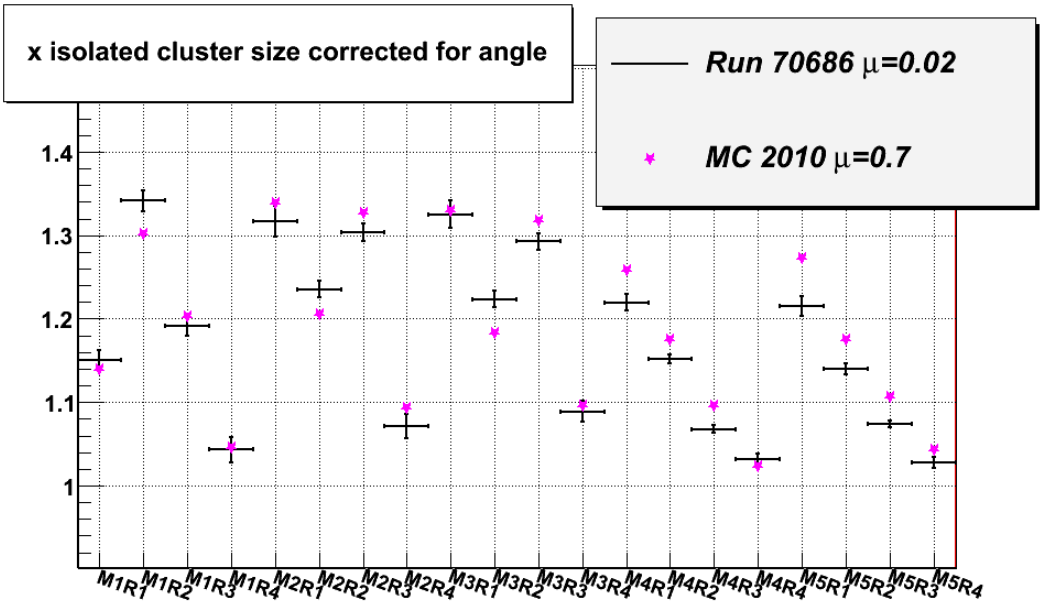

Figure 7 Average cluster size for track hits in data and MC2010. The effect of track angle is corrected for. To suppress the effect of pile–up, only isolated clusters and low–luminosity data are used.

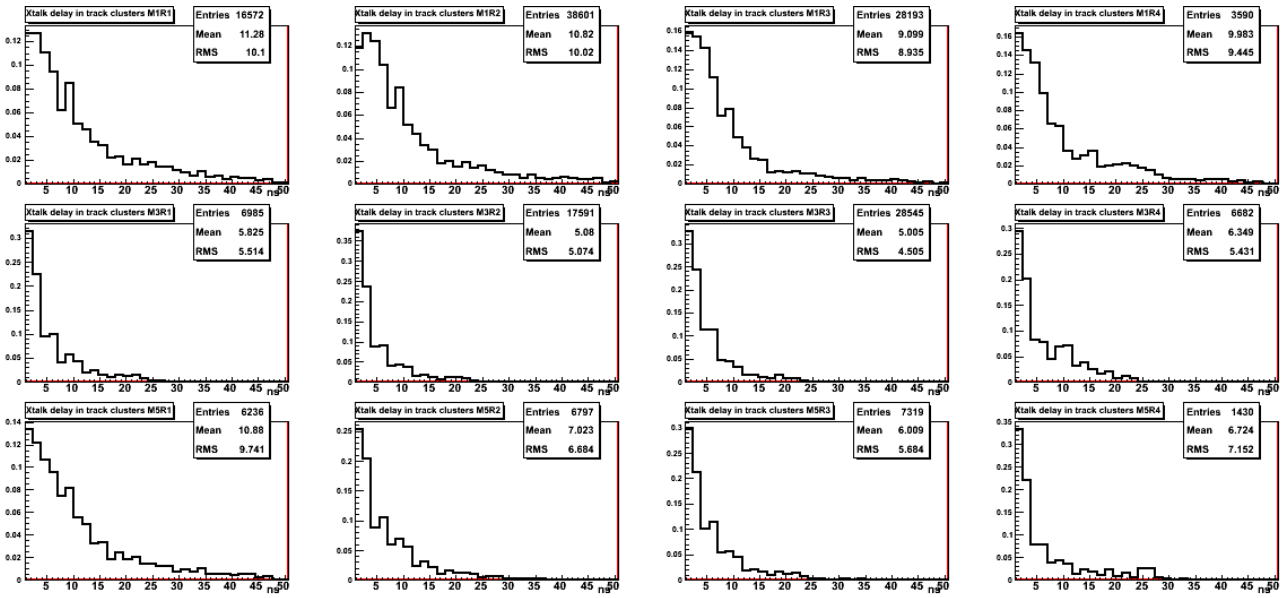

Figure 8 Time delay, in ns, of pads in track clusters with respect to the first in time for different detector regions. TAE events are used where the detector is read out in a gate of 125 ns around the collision. The structure around 10 ns is due to a feature of the TDC response [2]

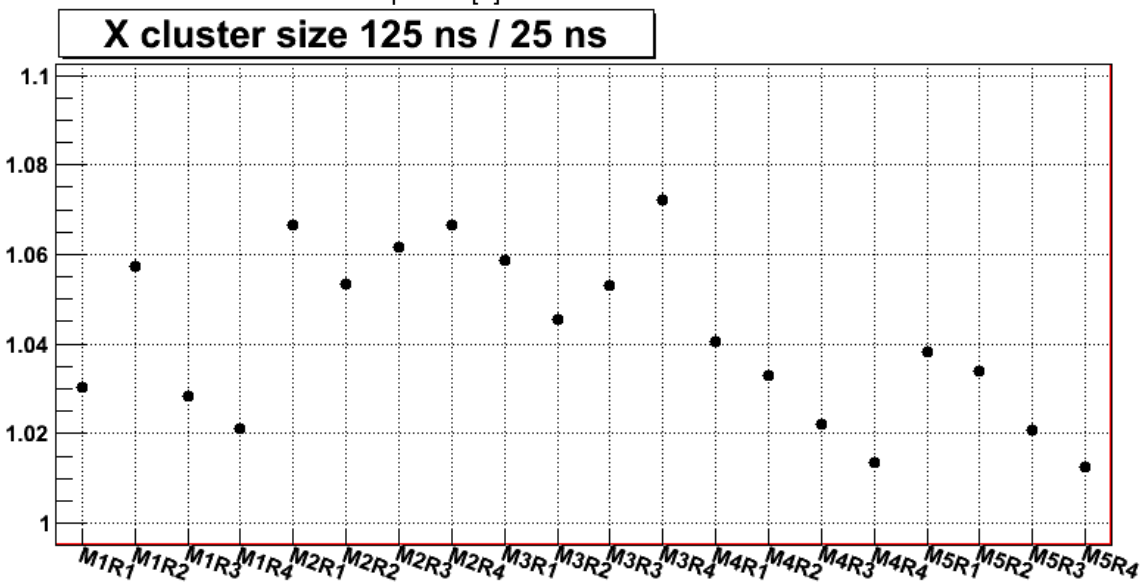

Figure 9 Ratio of cluster sizes along x for isolated tracks seen in a 125 ns time window to the ones in the nominal 25 ns window.

of the gain over threshold settings. The average cluster size does not exceed 1.35 in any region, a value well within the L0 trigger requirements[5].

The time structure of cross–talk can be studied using TAE data and the time reconstruction feature of the muon detector readout, equipped with a 4–bit TDC. The time difference of pads in clusters with respect to the first cluster pad time is plotted in figure 8. The cross–talk tail extends far beyond the $\pm$ 12.5 ns trigger gate around the collision, making the cluster size seen in the TAE 125 ns wide time window larger by 1 to 7 %, depending on the region, as shown in figure 9. The late cross-talk signals are not normally acquired and thus are not affecting the trigger performance, though contributing to background for future beam operations with 25 ns bunch spacing, and to dead time already with 50 ns bunch spacing.

5 Particle Rates

The rate capability was one of the key request for the choice of technology and design of the muon detector. Detailed simulations were developed [6] to evaluate the particle rates and radiation doses expected for the nominal LHCb operations at 14 TeV and luminosity of $2 \cdot 10^{32}$ Hz/cm^2. The detector was designed to stand a rate larger than a factor 3 (for M2–M5 stations) or 2 (for M1 station) with respect to these simulations, for the 10 years of planned LHCb operation. The 2010 data allowed to measure the actual rates at 7 TeV energy for a wide range of luminosities and to compare them with expectations.

The average number of firing logical pads per unit surface and triggered event $r_T = dN_h/dSdN_T$ was computed for every chamber. The average and maximum chamber rate was obtained for every detector region, after removing the few chambers with channels affected by some pathology (dead or noisy). From the rate seen by triggered events we intend to evaluate the rate of firing pads per visible interaction r_{vi}, by definition independent of luminosity, and the contribution not due to the triggered collision r_{bkg}, that could be due to spillover, beam background or detector effects (residual noise, late cross talk or afterpulses). For a given trigger T with efficiency ϵ_T we have in general

$$r_T = \frac{\sum_{n=0}^{\infty} P(n;\mu)(nr_{vi} + r_{bkg})\epsilon_T(n)}{\sum_{n=0}^{\infty} P(n;\mu)\epsilon_T(n)} \tag{2}$$

where n is the number of visible collisions in the event, μ its average value and P is the Poisson distribution. For triggers acquired randomly in collision bunches we have

$$r_{rnd} = r_{vi}\mu + r_{bkg} \tag{3}$$

while for an ideal Minimum Bias trigger

$$r_{MB} = r_{vi}p + r_{bkg} \tag{4}$$

where $p = \mu/(1 - P(0;\mu))$ is the pile–up factor.

Since the statistics for random triggers is very limited, the μbias trigger provides the least biased available trigger for this measurement. Figure 10 shows the ratio $r_{rnd}/r_{\mu\text{bias}}$ in the 20 detector regions for different levels of luminosity. In most cases, the ratio is very close to μ/p, demonstrating that the rates are dominated by the products of the triggered collisions. The only relevant deviations are observed at very low luminosity, where the residual noise is still relatively important, and for the outer part of the M5 station, where a relatively important contribution from back–scattering is expected due to the low rates in this region and the limited shielding at the back of the upper detector part. However, for the most illuminated regions (M1 station and region 1) the rate is expected to scale with luminosity.

We then extrapolate the rates from each sample run at nominal luminosity using the measured values of $r_{\mu\text{bias}}$ and p:

$$R = \frac{dN_h}{dSdt}\frac{\mathcal{L}_{nominal}}{\mathcal{L}} = r_{\mu\text{bias}} \times \frac{dN_{\mu\text{bias}}}{dt} \times \frac{\mathcal{L}_{nominal}}{\mathcal{L}} = r_{\mu\text{bias}} \times \frac{65mb}{p}\mathcal{L}_{nominal} \tag{5}$$

where we used the formula

$$\frac{dN_{\mu\text{bias}}}{dt} = 65\text{mb} \times \frac{\mathcal{L}}{p} \tag{6}$$

that was evaluated, with 10% uncertainty, from the first luminosity studies. The result is shown in figure 11. The scaling of rates is verified within a few percent across five order of magnitudes in luminosity. As anticipated, the

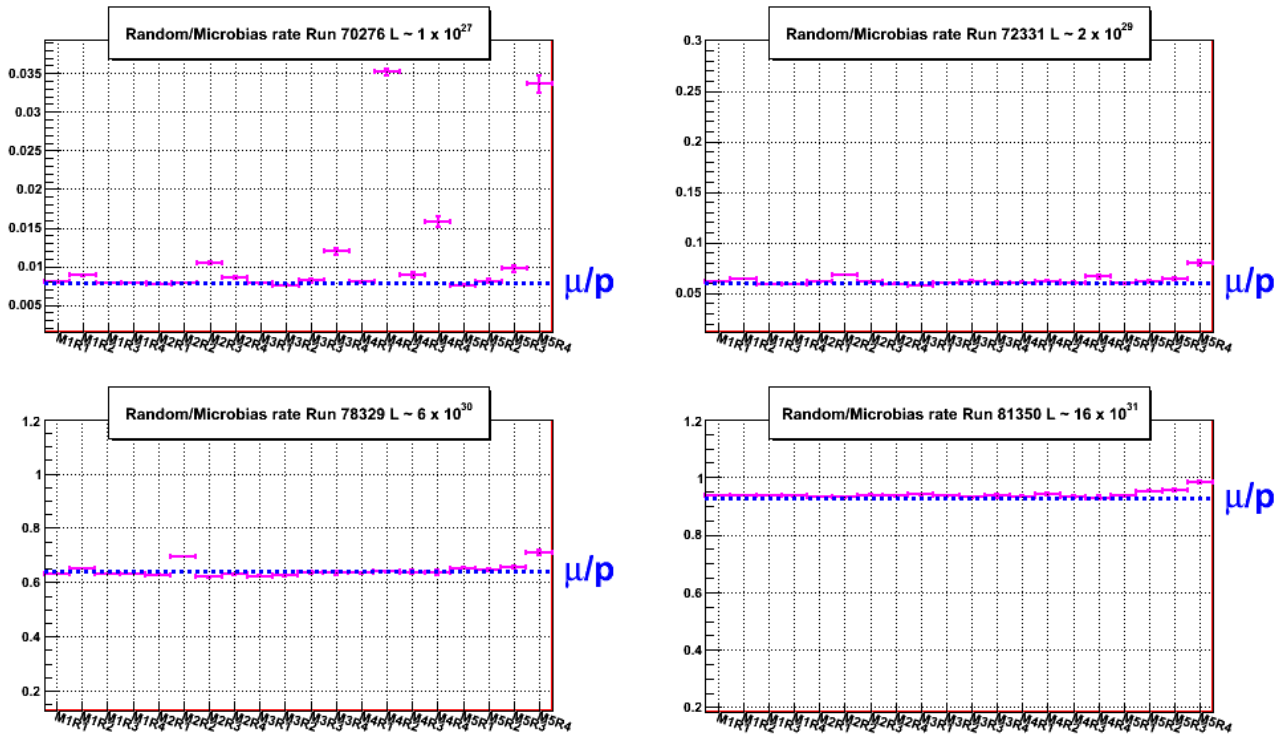

Figure 10 Ratio of muon rates seen in random and μbias events for some sample runs with different beam conditions.

only exception is the outer region of M5, where the contribution of backscattering depends on the beam conditions (μ and bunch spacing) of each run.

For the most irradiated region M1R1, equipped with GEM detectors, the average R value is found to be 60 kHz/cm^2. For the most irradiated chambers in regions M1R1 and M2R1 we find respectively 130 and 45 kHz/cm^2, as shown in fig. 12, where the minimum, average and maximum chamber rates in each region are reported. The errors shown on the plots are statistical only. As already mentioned, the global rate scale is affected by a 10% systematic uncertainty.

In figure 13 we compare the measured values of the average R in each region with the predicitons of two simulations: the MonteCarlo data previously mentioned, produced with the full GEANT simulation in the nominal LHCb configuration at 14 TeV including spillover, and more recent MonteCarlo data produced in the 2010 configuration at 7 TeV, not including spillover. The simulation at 7 TeV reasonably reproduces rates for the outer regions (except for the missing spillover contribution in M5), while underestimating them for the inner and M1 region by up to a factor 2, that is however within the design safety factor, as shown in figure 14.

The energy dependence of rates, using also the 2009 data at 0.9 and 2.3 TeV, is shown in figure 15.

The contribution of spillover or delayed hits can be estimated from TAE events. We use in this case L0MB events, since the μbias triggers were not available in the TAE mode. For the M5R4 region, most affected by backscattering, the rate increases by a factor 10 (from 1.5 to 15 Hz/cm^2). The ratio of total rate to in–time rate (within the normal 25 ns gate), is shown on fig. 16 for the other regions. The contribution due to late cross talk signals was estimated in the previous section [a]. After subtracting it, the rate increases by 5–10% in M1 and around 40% in M2–M5 stations. This is an upper limit on the rate of spillover particles, that are expected to produce larger cluster sizes than in–time particles. The space distribution of such late signals, normalized to the in–time pad distribution, is shown on fig 17. Cross–talk is expected to contribute with an uniform factor within each region. The plots show some excess of late hits, clearly not related to the intime ones, in some particular positions, notably the upper part of the M5 station and the outer corners, due to the limited shielding from backscattered particles.
The extra rate is mostly seen in the 25 ns following the bunch crossing, as shown in figure 18.

[a] note that on fig. 9 we showed the increase due to late signals of the cluster size along x. We need to consider here the total cluster size for which the effect is larger, since multiple signals in both x and y views produce ambiguities overmeasuring the cluster size.

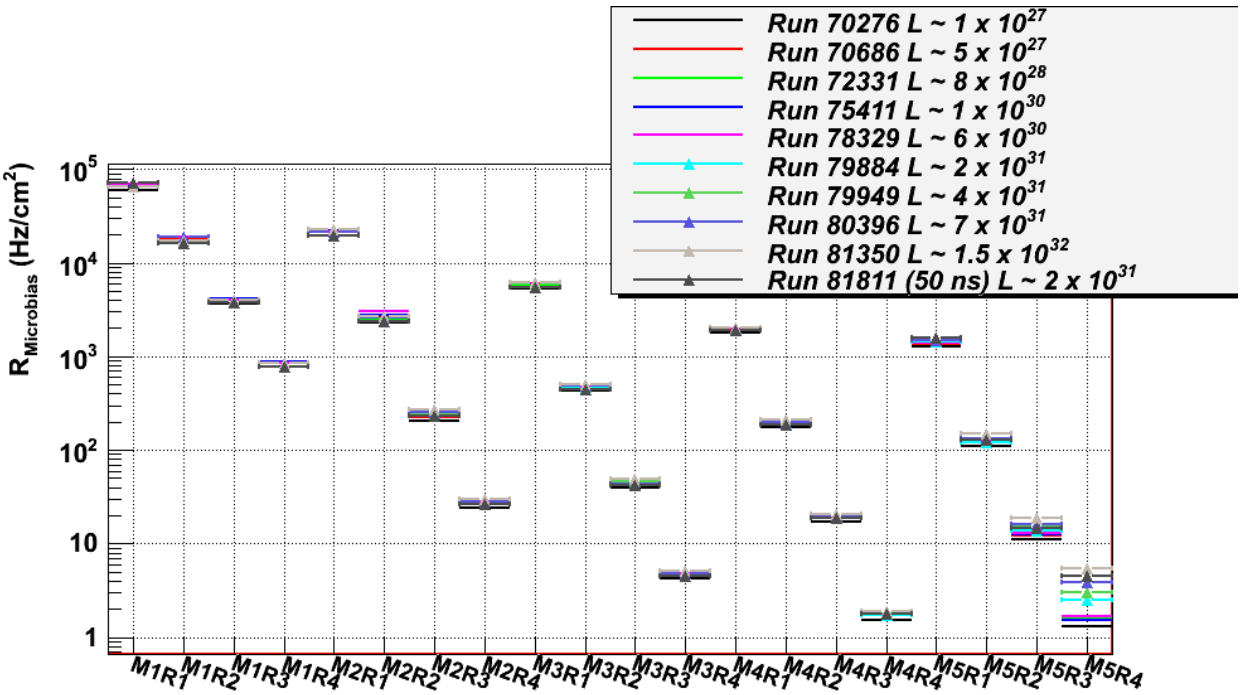

Figure 11 Average rate, extrapolated at the nominal luminosity, in the 20 muon detector regions for each of the 2010 sample runs of table 3.

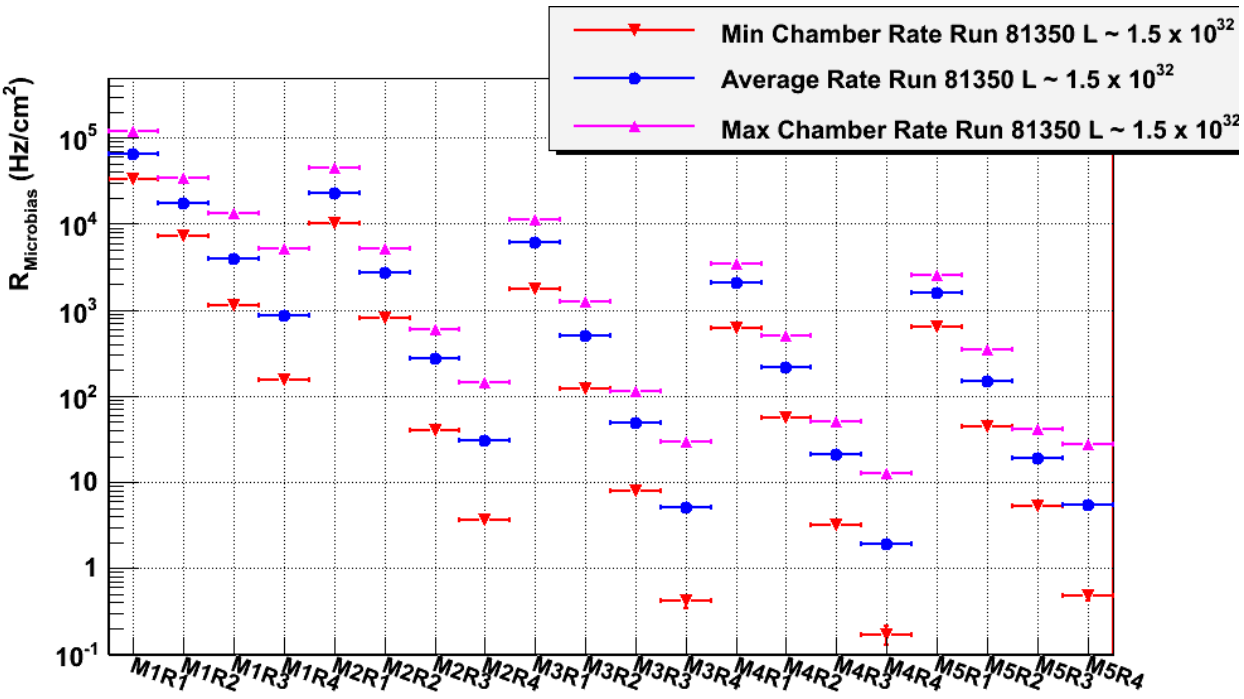

Figure 12 Maximum, minimum and average chamber rates for the 20 muon detector regions.

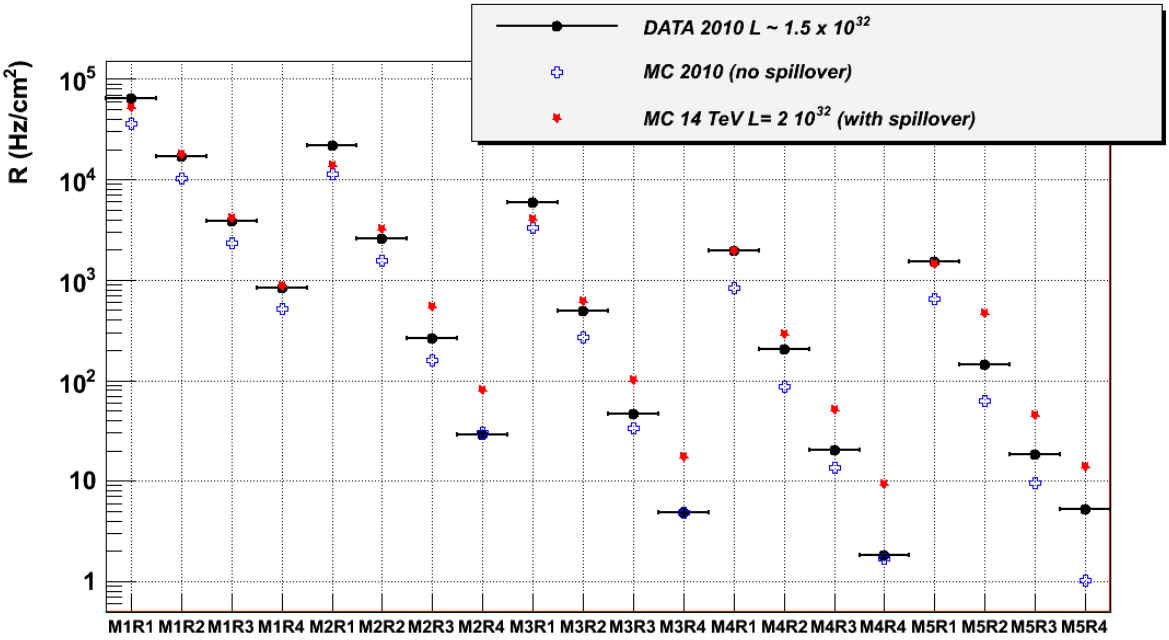

Figure 13 Comparison of the rates seen in 2010 data with the MC data produced in the 2010 configuration at 7 TeV, and the more detailed simulation used in the detector design phase.

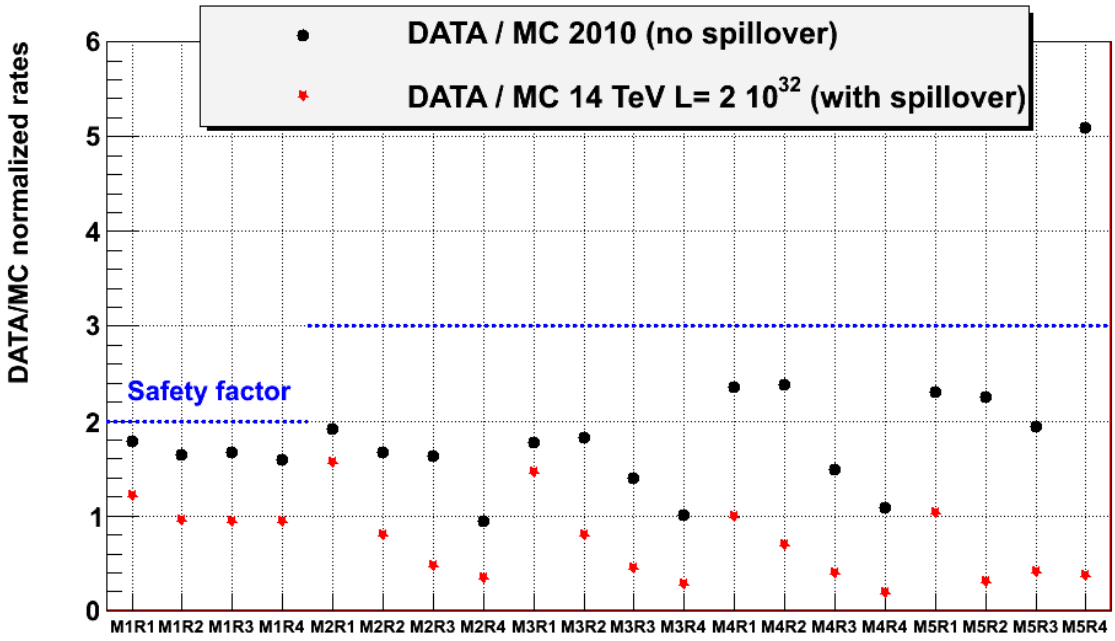

Figure 14 Ratio of the rates seen in 2010 data to the MC predictions.

Finally, we check for possible sources of particles outside collision events. In figure 19 we compare the rates seen in beam–beam, empty–beam and empty–empty randomly triggered events. Except for the low–rate external regions of M5, rates outside collisions are less than 10% smaller than collision rates. The rates seen in empty–empty events are dominated by the delayed hits from the collisions in the previous bunches, as shown on fig.20. Most signals are seen in the 25 ns following a beam–beam event, though a small second peak at about 100 ns from collisions is also observed, that is expected from a known effect of afterpulse signals. The rate level far from bunch trains is compatible with the residual detector noise. No evidence for relevant beam backgrounds is thus observed.

5.1 Occupancy

During the 2010 run the detector was operated with μ values up to 2.7, more than five times larger than the nominal pile–up level. The resulting detector occupancy for μbias triggered events with different μ values is plotted in figure 21. The bottleneck in the muon readout chain is the output bandwith of the TELL1 boards reading out the M1 station data. As shown on figure 22, the hard limit of 450 bytes per event with 1 MHz L0 readout is expected to be reached only for $\mu \sim 4$, a value not foreseen for future operations.

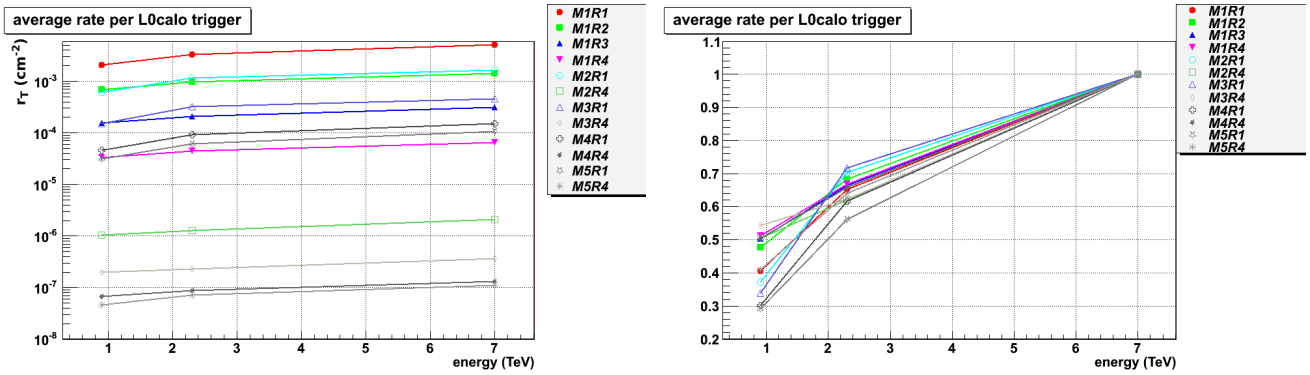

Figure 15 Muon rates for the 3 different c.m. energies available in 2009 and 2010 data are compared on the left plot. On the right plot, the same numbers are normalized to 7 TeV and shown on linear scale.

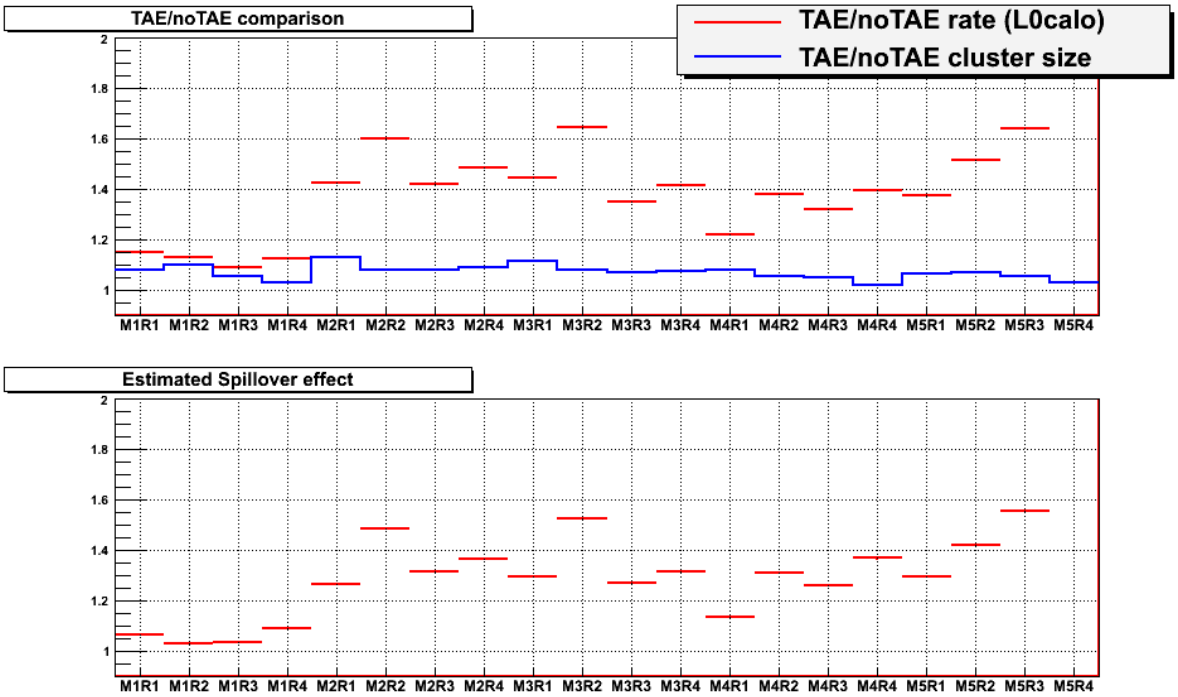

Figure 16 The ratio of the rate in 125 ns time window to the rate in 25 ns is shown on the upper plot, together with the ratio of total cluster sizes for track hits. The lower plot shows the ratio of the two upper curves, estimating the contribution to rates from spillover particles.

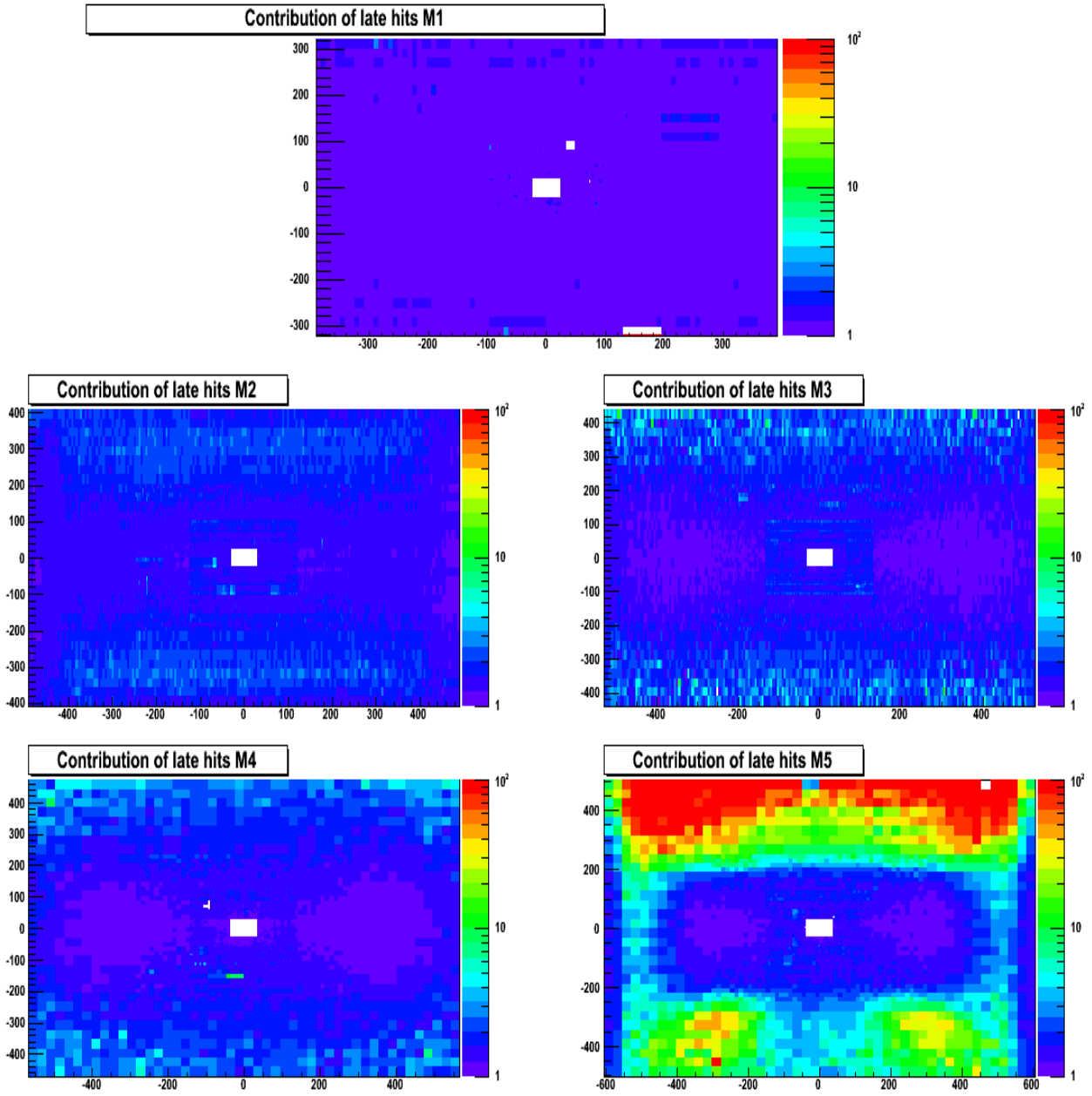

Figure 17 Space distribution of the ratio between the rates in 125 ns and 25 ns. The contribution of late hits from backscattering is evident in the outer regions, notably for station M5.

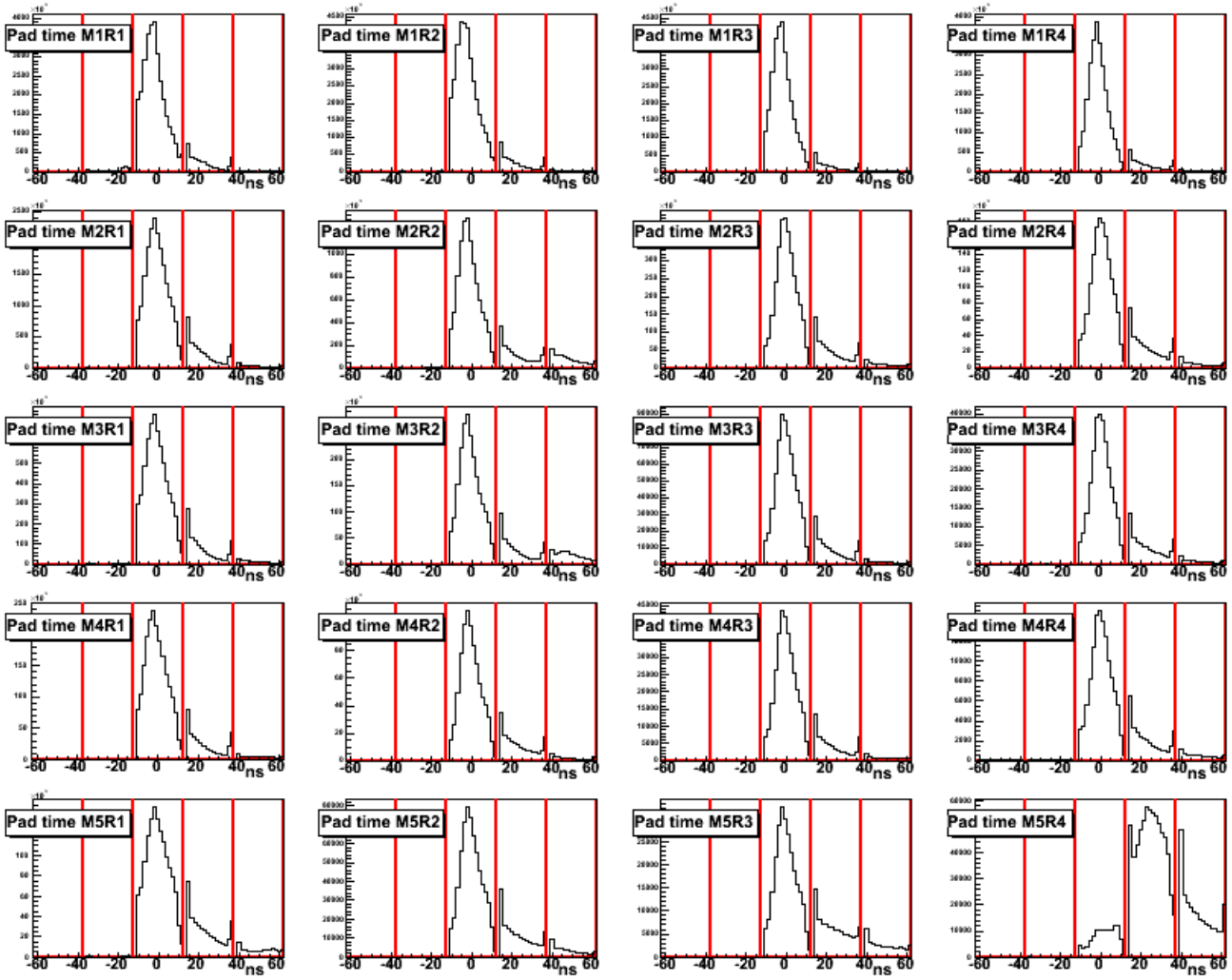

Figure 18 Time spectrum of the muon detector signals in the 20 detector regions from TAE events. The red vertical lines indicate the boundaries between consecutive 25 ns gates. Only the central one is normally acquired. The structures at the gate boundaries are due to a feature of the TDC reading the fine time inside the 25 ns gate.

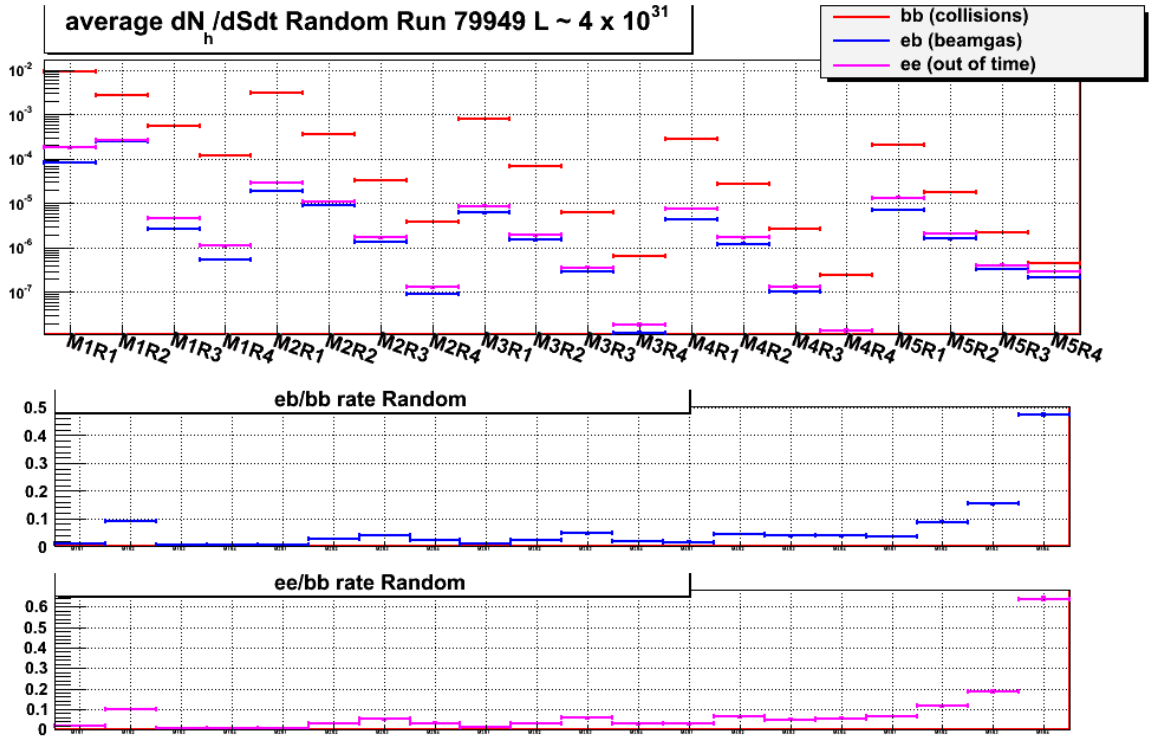

Figure 19 Comparison of rates seen in events with beam–beam crossing (bb), single beam (eb) and no beams (ee).

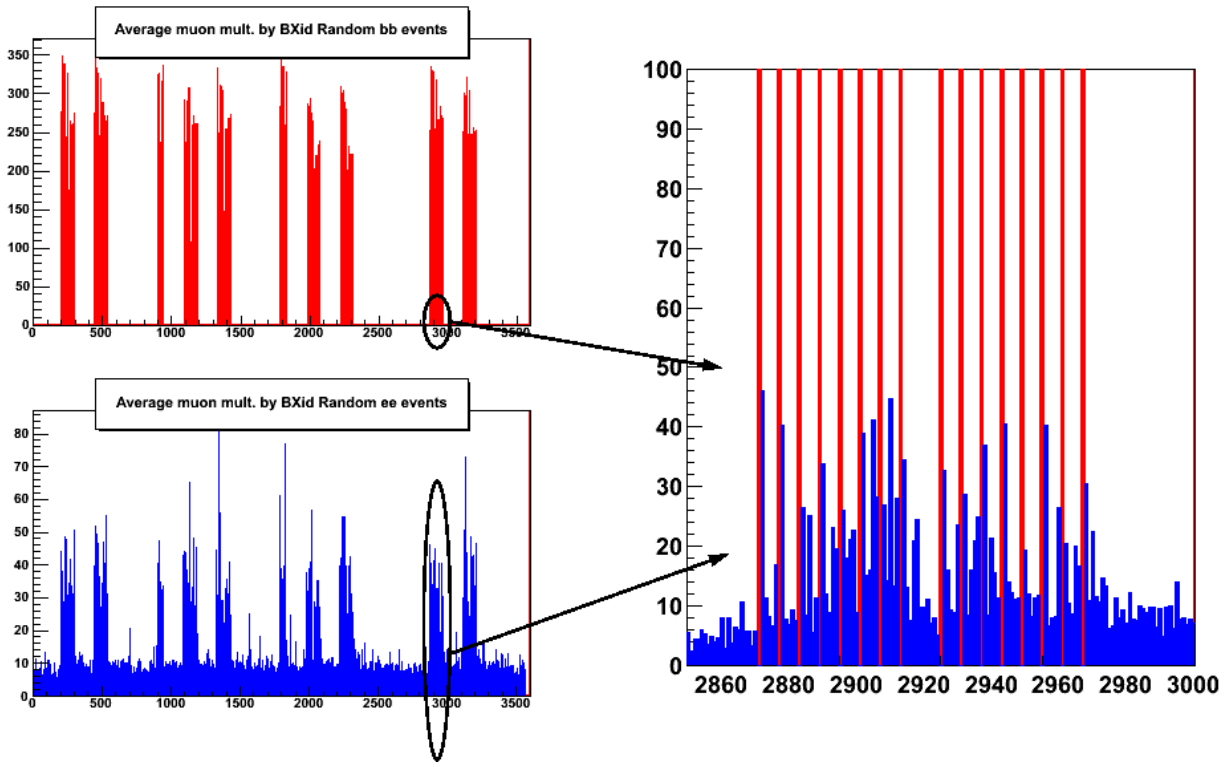

Figure 20 The muon detector pad multiplicity is plotted as a function of the bunch counter within the LHC orbit for beam–beam events (upper left) and empty events (lower left). It is clear that the activity seen in empty–empty events is related to collisions of previous bunches, as can be clearly seen in the right plot, showing the details of a bunch train.

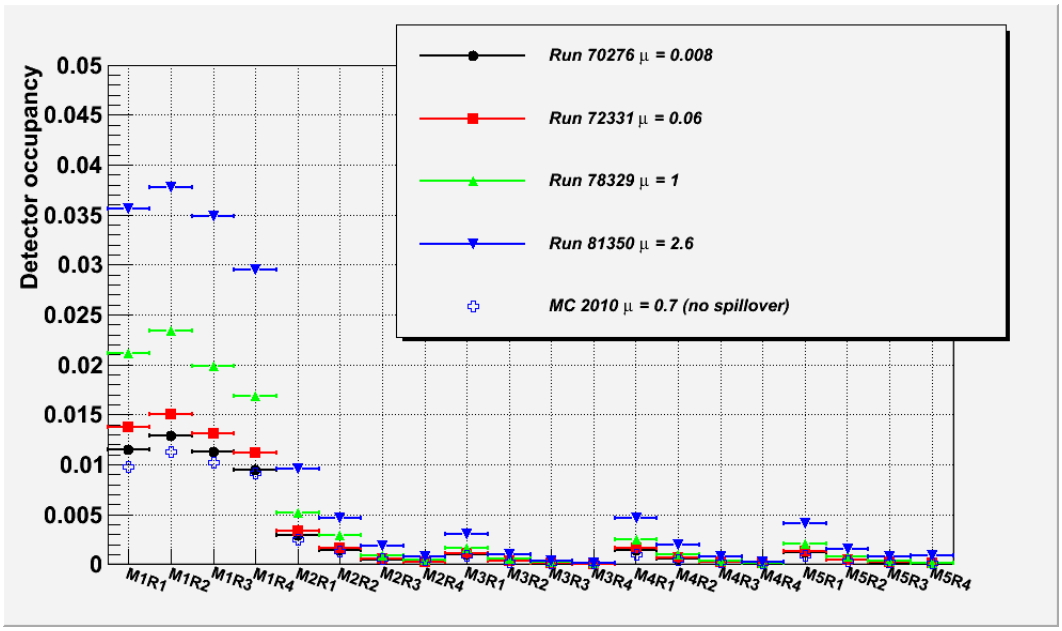

Figure 21 Average occupancy of the muon detector (in terms of logical pads) for μbias triggered events with different μ values. Predictions from the 2010 MonteCarlo data at $\mu = 0.7$ are also shown for comparison.

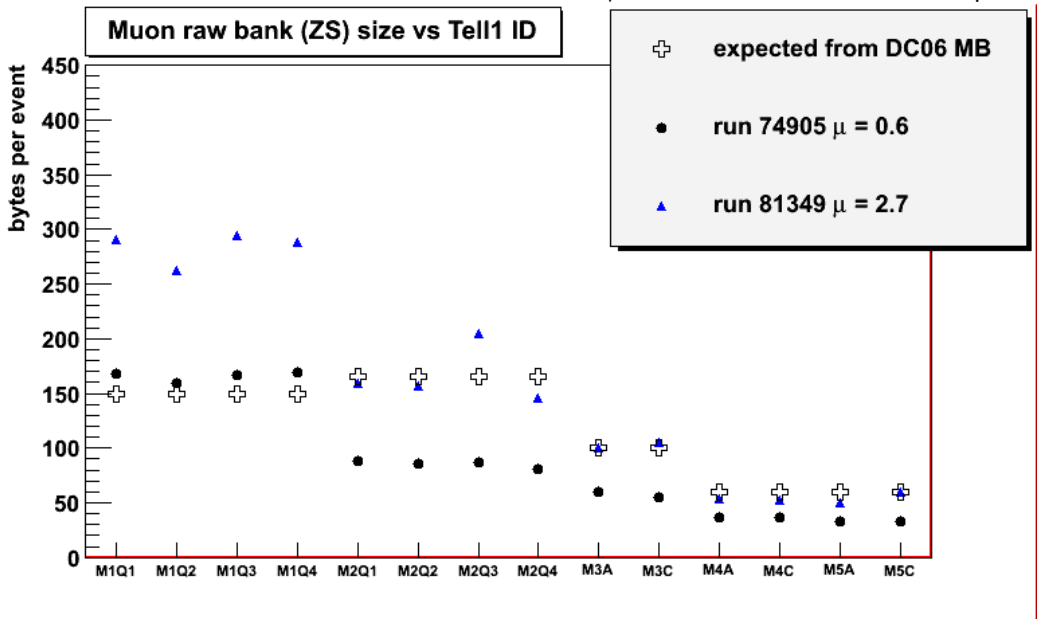

Figure 22 Average size of the output of each muon TELL1 board for different μ values, in units of bytes for L0–triggered event. The expectation based on minimum bias events simulated with the DC06 MonteCarlo is shown for comparison. For the maximum L0 rate of 1MHz, the TELL1 bandwith hard limit is 450 bytes per event.

6 Timing

A muon track can be triggered by the L0 muon trigger only if a hit is recorded in each of the five stations within the 25 ns LHC gate associated to a beam–beam crossing. This timing constraint is the most stringent requirement for achieving the design 95% muon detection efficiency. To reach this goal, the detectors were conceived to have a time resolution better than 4 ns at their nominal settings, while the 120k readout channels have to be time–aligned at the 1 ns r.m.s. level. Though, tails in the time response are expected to be one of the main sources of detector inefficiency.

The time alignment of the detector has been achieved in several steps. Test signals produced by a custom pulser system were used for a first equalization. Cosmic data collected in 2009 allowed to refine the intercalibration using physical signals. These two steps are described in detail in [2] and [7]. The first data collected by the experiment with LHC beams allowed for a further refinement of the alignment, improving the intercalibration for the regions with limited statistics of cosmic events, and fixing the absolute alignment with respect to the 40 MHz LHCb clock in synchronism with the beam collisions. Finally, the residual inefficiency due to the finite timing resolution could be estimated.

6.1 Refinement of the time alignment

After the calibration with cosmic data, a satisfactory time resolution was reached for all regions except the most inner ones, and notably M1R1, where the statistics was still a limit. The precise timing of beam particles allowed to quickly intercalibrate the channels of the most illuminated regions, i.e. the M1 station and the highly segmented R1 regions, using data from the short 2009 run. For the other regions, only a few channels exhibiting an anomalous shift in the time response due to some hardware interventions were identified and fixed, also using a sample of cosmic data acquired just before the start of the 2010 run. Thus, the combined use of cosmics and first beam particles allowed to reach a close to final timing intercalibration already before the start of the 2010 data taking.

The detector efficiency could then be optimized by tuning the time offset with respect to the 40 MHz LHCb clock. The single channel time distribution exhibits an asymmetric shape, with a longer tail for late times, due to:

- the intrinsic chamber response (nonlinear dependence on drift path and pulse height);
- the effect of delayed cross–talk hits, introducing the tail shown in figure 8;
- the effect of nonprojectivity, notably for low momentum tracks receiving a relevant momentum kick from the magnet, causing a delay up to 2 ns due to longer track trajectories with respect to the projective case.

This suggests that, in order to minimize the fraction of signals falling outside the 25 ns gate, the average time should not be centered on the middle of the DAQ gate, but slightly before. The optimal offset is region dependent as is the shape of the time spectrum. Moreover, offsets among regions were already introduced by the optimization of the HV and threshold settings (a common HV value of 2.65 kV for all regions, and high thresholds, were used for the 2009 cosmic data taking), and a small ($\pm$ 2 ns) systematic region–dependent bias was also expected from the cosmic calibration. [b].

In conclusion, the offset needed to be optimized independently for every detector region. Unfortunately, the tails of the time spectrum could not be measured precisely using the SYNC TDC, since its response is nonlinear at the gate boundaries. Instead, some special runs were acquired in TAE mode, varying the global time offset in steps of 1 ns. For every data sample, standalone muon tracks were reconstructed requiring hits in all five stations. The optimal offset was chosen by maximizing the timing efficiency, defined as the probability that at least one of the track hits in a given station is found within the central 25 ns gate. The timing efficiency was measured for each detector region using L0MB triggered events. The result of this scan is shown in figure 23. The optimal offset for each region was obtained from a parabolic fit of the timing efficiency values and ranges from 0 to -4 ns.

The corresponding maximum values of such efficiency were found to be at least 98.5% for all regions but M1R1. This value, already satisfactory, is a lower limit for the timing efficiency since fake tracks from combinatorial backgrounds can still be present in the track sample. As will be discussed on the next sections, this background can be suppressed through tight quality cuts that are not possible with the limited statistics of the timing scan

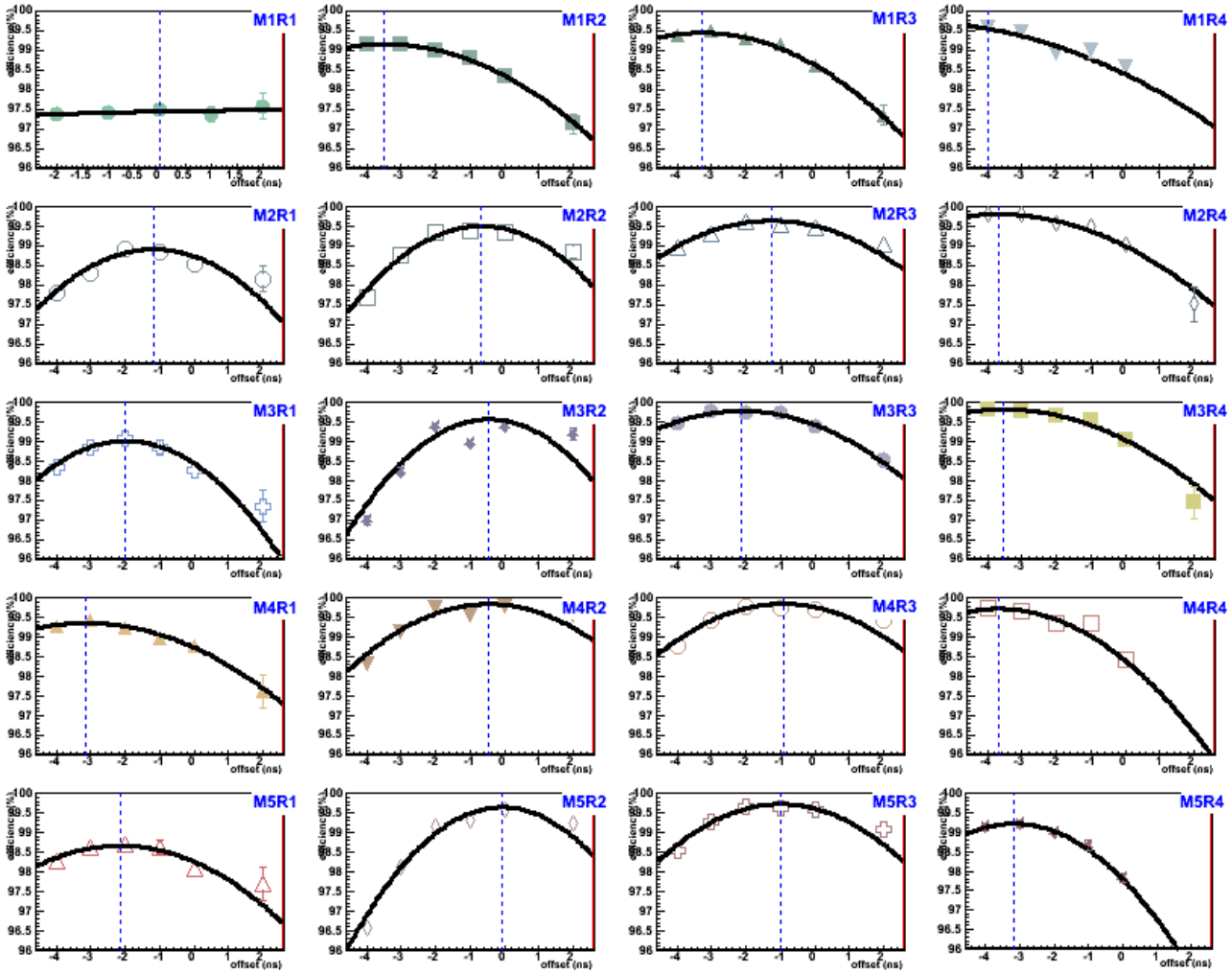

Figure 23 Results of the time scan performed in the first days of the 2010 run to optimize the time offset of each muon detector region. The timing efficiency is plotted against the global time offset applied to the LHCb trigger signal received by the muon detector.

data. However, the small background contribution is expected to be flat in time and should not affect the position of the maxima of figure 23.

The residual inefficiency in the M1R1 region was found to be still partly due to internal misalignment, particularly for 3 GEM chambers, due to some change in the HV settings with respect to the 2009 data. The intercalibration was improved using the first collected physics runs. The new constants were applied since may 28th 2010.

6.2 Timing Performance

After applying the optimal time offsets and the improvements to the intercalibration, the detector performance could be verified using some special TAE runs by estimating the time resolution and, most importantly, the timing efficiency for each detector region.

Two TAE samples were available:

- run 70493 was aquired at the beginning of the physics data taking, before applying the final intercalibration for region M1R1. Events were triggered by L0MB;
- runs 81740–81745 were acquired at the very end of physics data taking. In this case the L0MB triggers were downscaled by a factor 100 and an adequate statistics was available only using the physics L0 triggers based on calorimeters (electron, photon, hadron triggers).

As will be discussed in more detail on section 7.1 for the measurement of total efficiency, tight requirements are needed, particularly for station M1, in order to reach a purity of the sample of standalone muon tracks well above the expected efficiency of ~ 99 %. However, the limited statistics of TAE data did not allow to select muons from J/ψ, and also the quality cuts used for measuring the total efficiency of stations M2–M5, discussed on section 7.1, had to be relaxed.

TAE events were fully reconstructed so that standalone muon tracks (Mtracks) could be required to have a good matching with a long or downstream track reconstructed by the tracking detectors (Ttrack) having a momentum larger than 8 GeV/c to ensure that tracks have an adequate range to reach the M5 station. The distance in X and Y between the Ttrack extrapolation and every cluster of the Mtrack was required to be lower than 3 standard deviations, where the r.m.s. of the distance distribution was calibrated as a function of the TTrack momentum and detector region using the data themselves. An isolation requirement was also set on Mtracks, rejecting candidates where clusters not belonging to the Mtrack were found within 1 standard deviation from the Ttrack extrapolation. The distance between Ttracks and the inner and outer borders of the detector volume was required to be larger than 13 cm in M2–M5 and 11 cm in M1.
Clusters inside the five chambers with pathologic behaviour mentioned on section 2.2, namely M1A22C, M1A24C, M1A16A2, M4C19A3 and M3A16A3, were not considered for the timing efficiency calculation.

The time spectrum of the most centered track hit on every station is shown on fig. 24. Table 4 reports the resulting timing efficiency in each detector region for the final TAE sample. From the sensitivity of the measured values on the quality cuts, we can expect the efficiency to be still sistematically underestimated by a few per mill in the regions most affected by combinatorial background, namely region 1 and stations 1 and 5. Nevertheless, the overall timing efficiency, namely the probability that a track has a in–time signal in all five stations, was measured to be 98.83 ± 0.09 %, a value well beyond requirements. The corresponding core time resolution is shown on fig. 25, where the time distributions are fitted with a gaussian around their maximum. Values between 3 and 4 ns are measured, in line with expectations.

The comparison of the two TAE samples is shown in fig. 26. Despite the different triggers, resulting in a different momentum spectrum and space distribution of the tracks, the timing performance was found to be in very good agreement, except for region M1R1 where a more accurate intercalibration was used for the second sample. The result demonstrates the excellent stability of the muon system along the 2010 run.

[b] in the absence of an external time reference, only the first hit in time for every cluster was used, introducing an effect depending on the average cluster size

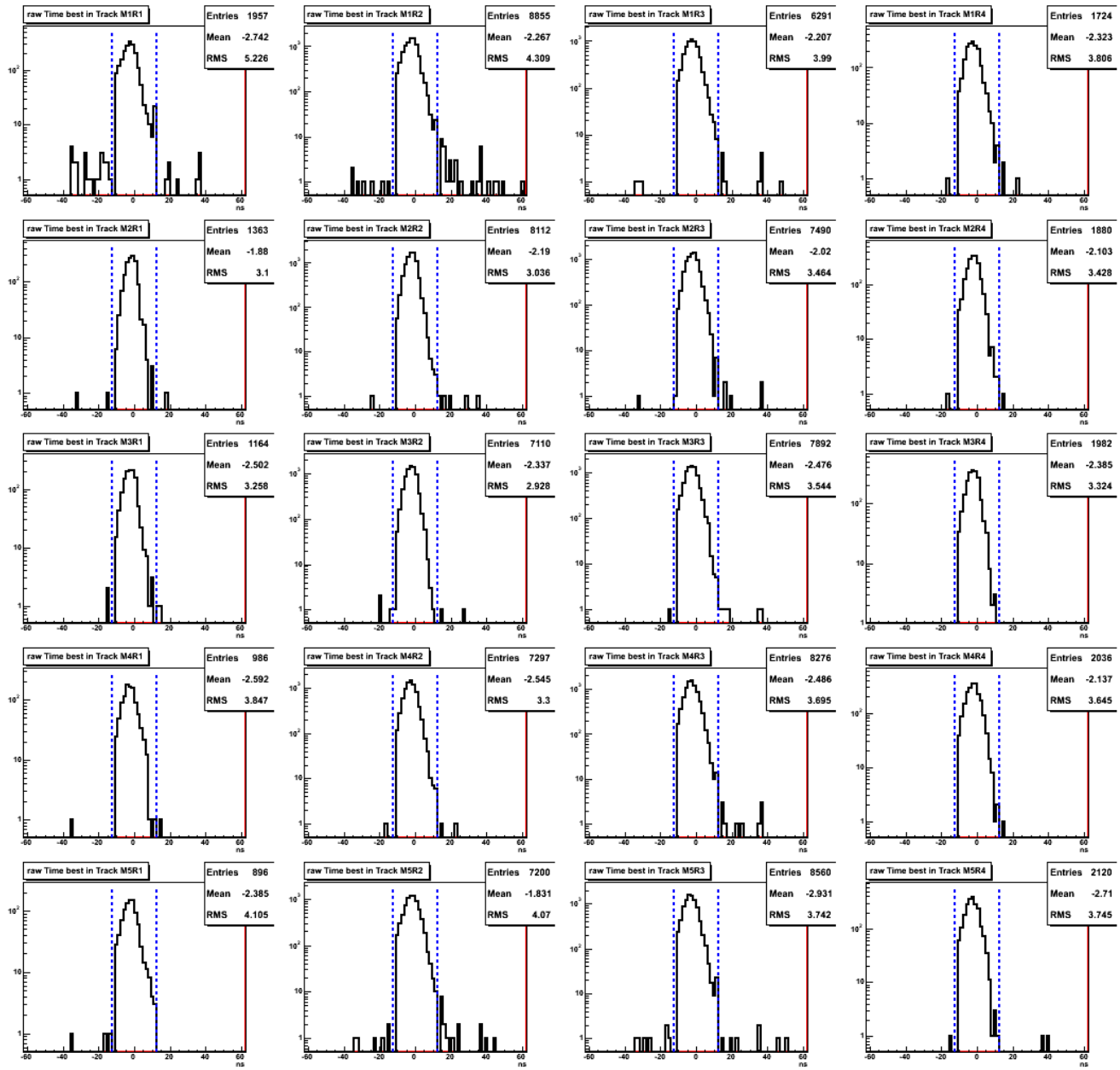

Figure 24 Time distributions of the “best” (most time centered) track hit per station for TAE runs 81740–5. The y scale is logarithmic to show the tails of the time response. The vertical lines show the boundary of the central 25 ns gate. For regions where the logical pads are obtained crossing two logical channels, the average of the two times is used (though both signals are required to be in the central gate for computing the timing efficiency).

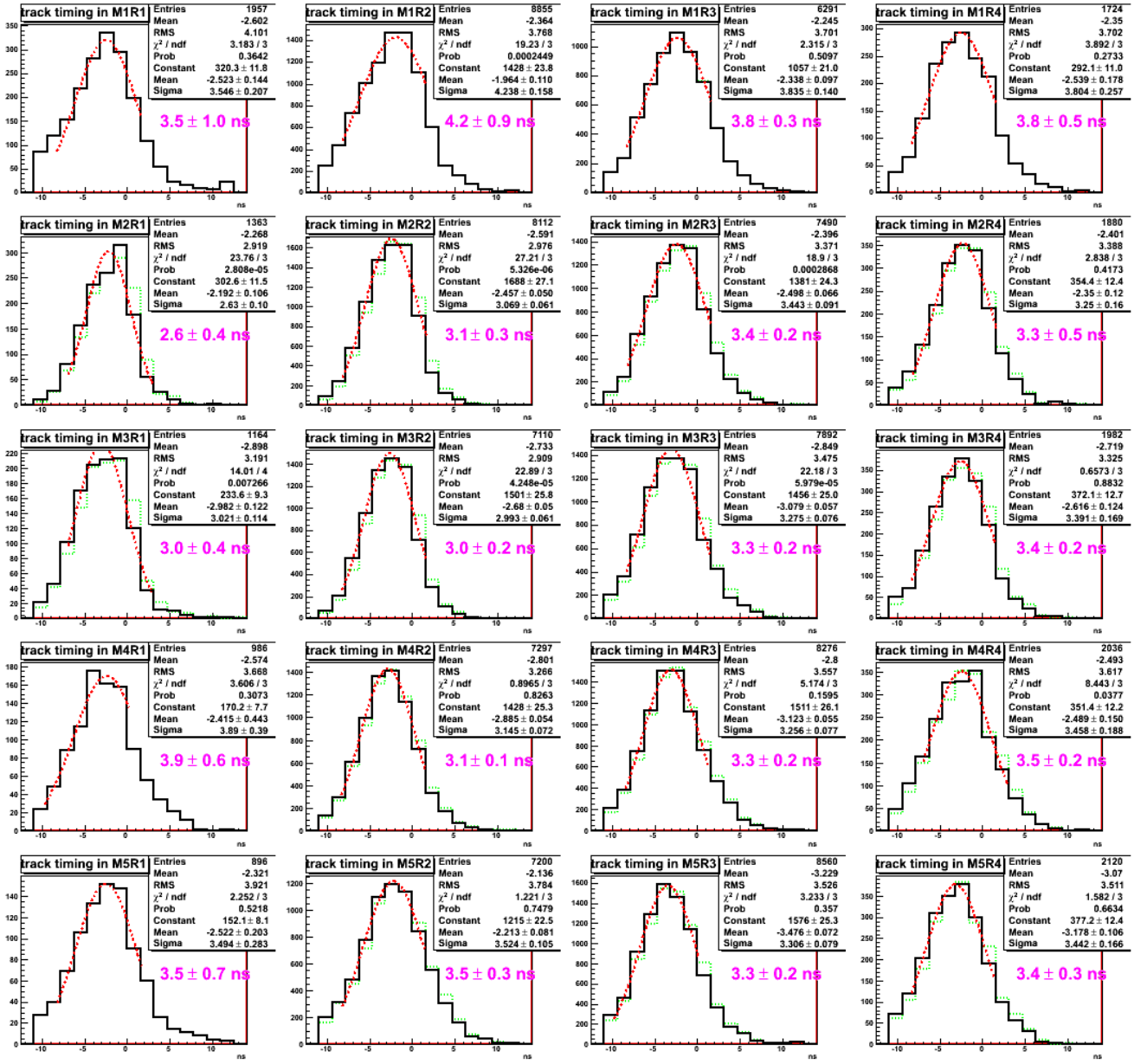

Figure 25 Detector time resolution per region for TAE runs 81740–5. The raw time distribution (dotted green lines) are corrected for the small effect of non–projectivity. The resulting histograms (black solid lines) are fitted with a gaussian in a 10 ns wide interval around the peak. The resolution is shown beside each plot. The error is mainly systematic, estimated varying the fit range.

Table 4 Timing efficiency, in per cent, for each detector region, obtained from TAE runs 81740–5. The average values by station are also reported.

Station	Average	R1	R2	R3	R4
M1	99.48± 0.07	98.4 ± 0.4	99.50 ± 0.10	99.78 ± 0.10	99.77 ± 0.26
M2	99.79± 0.05	99.6 ± 0.4	99.72 ± 0.09	99.91 ± 0.07	99.89 ± 0.21
M3	99.82± 0.04	99.5 ± 0.4	99.72 ± 0.09	99.91 ± 0.06	100.00 ± 0.17
M4	99.91± 0.03	99.8 ± 0.4	99.96 ± 0.06	99.88 ± 0.07	99.95 ± 0.18
M5	99.75± 0.05	99.7 ± 0.5	99.67 ± 0.10	99.84 ± 0.07	99.86 ± 0.20

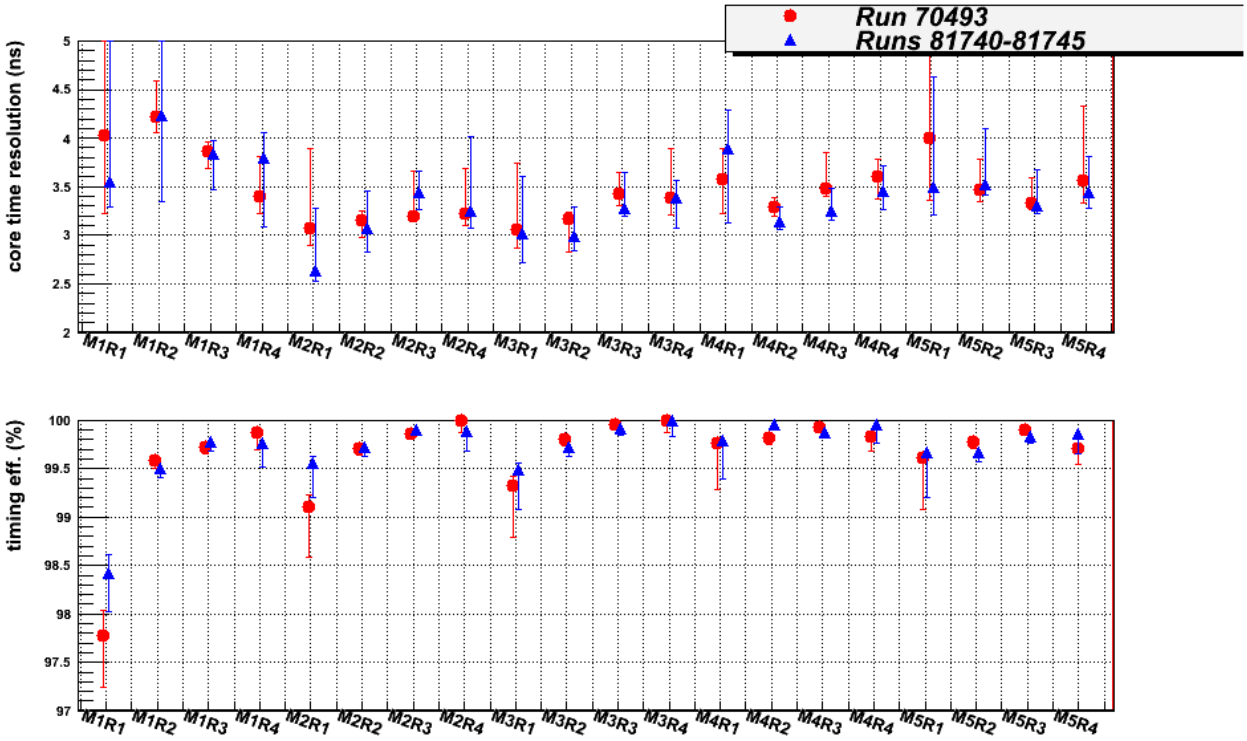

Figure 26 Comparison of timing performance as measured in the two TAE samples acquired before (april 21) and after (october 31) the bulk of 2010 LHCb physics data.

6.3 Stability of the time response

The stability of the absolute time scale in the long term is affected by two effects:

- the LHCb clock drifts with temperature; variations were compensated manually during the run in order to be stable within ± 0.5 ns;
- variations of temperature and atmospheric pressure at the pit affect the gain of our chambers producing a time walk effect. The largest effect was expected from pressure variations, and was estimated to be equivalent to a ∼ ± 20V change in HV [8], corresponding to ∼ ± 0.4 ns.

We conclude that the time response can be assumed to be stable within ± 1 ns. To verify that such level of timing stability is actually achieved, we measured the average time of track hits as a function of time along the 2010 run using the sample runs of table 3. The result is shown in figure 27 for different detector regions. Variations at the level of ± 1 ns, clearly correlated among regions, are observed. This is compatible with the mentioned expected effects of LHCb clock time drift and chamber gain variation with atmospheric pressure. In order to spot possible uncorrelated effects, we show in figure 28 the variations of average hit time T with respect to a central run (taken at time t_0) and to region M5R4:

$$\Delta T_r(t) = \overline{T}_r(t) - \overline{T}_r(t_0) - \left[\overline{T}_{M5R4}(t) - \overline{T}_{M5R4}(t_0)\right] \quad (7)$$

All variations are compatible with zero, except for the 1 ns step observed for region M5R2. This is due to the change of the HV value for this region mentioned on section2.1, when the resulting time walk was only partially compensated for technical reasons. There is no evidence for a dependence of the time drift on the detector illumination, that could be a hint for an ageing effect on the chamber gain.

From the profiles of the time scan of figure 23 we can argue that the detector efficiency is expected to be stable within $\pm 0.2\%$ in all regions for time drifts within $\pm$ 1 ns.

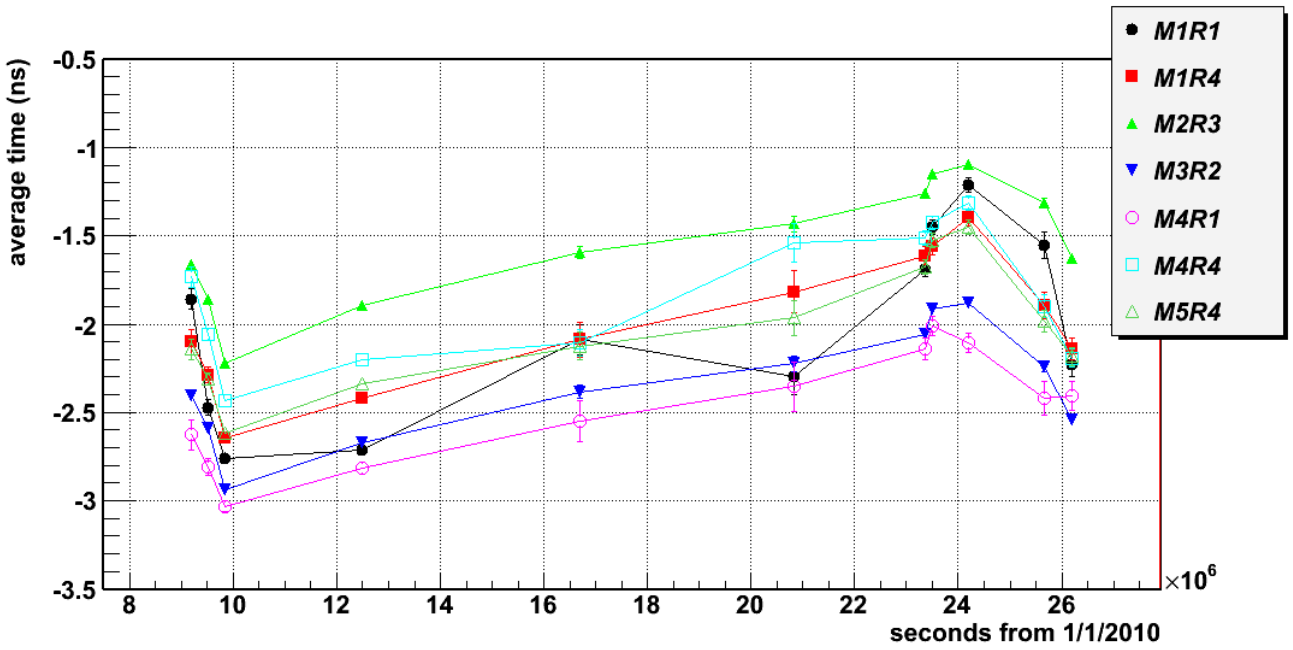

Figure 27 Variation of muon chambers time response along the 2010 run. The average time of the most time centered track hit in each station is plotted for each run of table 3, sampling the whole 2010 data–taking. The values for optimal efficiency depend on the detector region and have been fixed at the start of the run. Variations along the 7 months of operation do not exceed the $\pm$ 1 ns range.

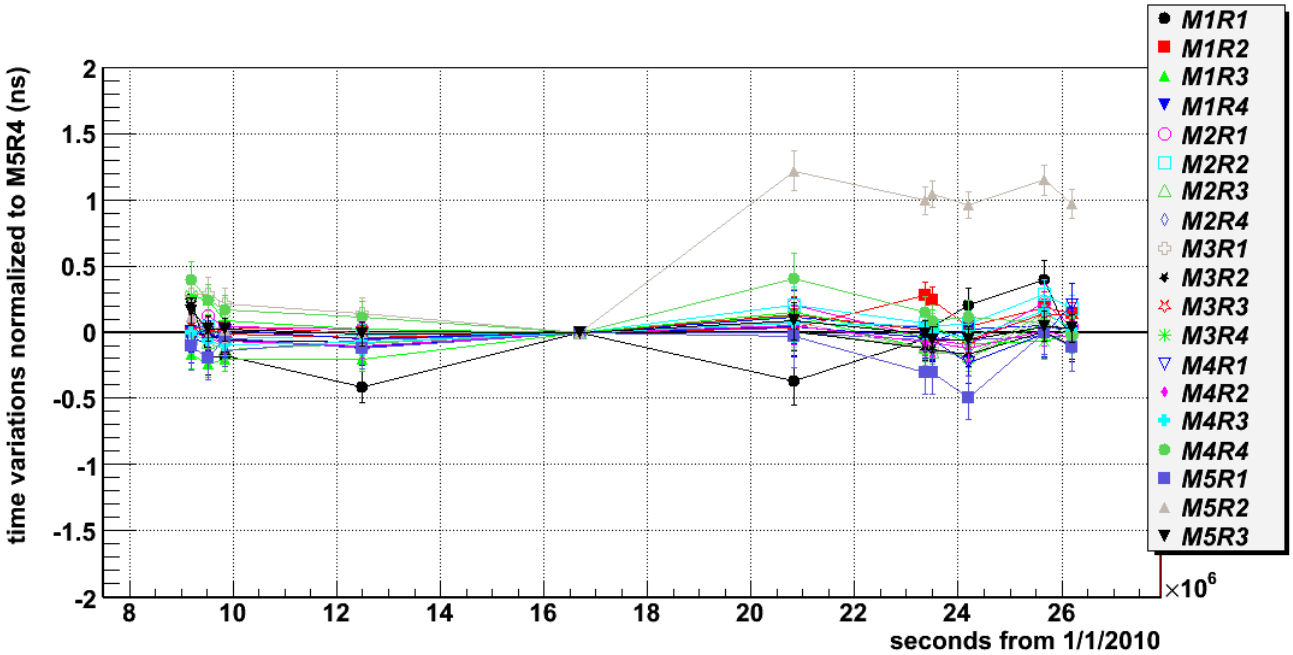

Figure 28 The variation of average response time is plotted here with respect to a sample run (78329) and to reference region M5R4, for the other 19 detector regions.

7 Efficiency

The overall performance of the muon detector is quantified by the detection efficiency of muon tracks when the system is operated in the standard data taking conditions. The aim is to evaluate the intrinsic efficiency of the system for each region of the muon detector, applying strict fiducial volume cuts and eliminating the few small zones where known problems are present.

For every station, we evaluate the efficiency using unbiased standalone [10] muon tracks (Mtracks) reconstructed using the other four stations.

7.1 Track selection

A tight selection is needed to improve the purity of the Mtracks in order to reduce the background to a level which is adequate for the efficiency measurement. Different procedures are applied to evaluate the efficiency of M1 and for M2-M5 stations.

For the analysis of M2-M5 stations, the Mtrack is validated by requiring the existence of at least one Ttrack matching within one sigma, both in X and Y, the clusters associated to the Mtrack in each of the four stations used for the fit. The X and Y values of the sigma are estimated by a gaussian fit to the central peak of the distributions of the distance between all the Ttrack predictions and the cluster positions in x and y projections respectively. Examples of these distributions for M1, M2, M3 and M5 stations, i.e. where the efficiency of M4 is being measured, are shown in fig 29, 30, 31 and 32.

Furthermore a lower cut at 12 GeV/c is applied on the reconstructed momentum of the Ttrack when M2 is the analyzed station and of 15 GeV/c for M3, M4 and M5 stations. In the cases where more than one Ttrack matches the Mtrack candidate according to the criteria listed above, and at least one of them has a momentum below the cut, the candidate is rejected.

A few specific additional cuts are applied. In evaluating M2 and M3 efficiency, where the occupancy is relatively higher, in order to avoid accidental combination with fake pads, the Mtrack candidate is rejected if in one or more Trigger Sectors lying within $\pm$ 8 σ_x or within $\pm$ 8 σ_y from the prediction, there is more than one channel hit in X and Y[c]. The reason for this tolerance and the values of σ_x and σ_y will be discussed in the following sections. When analyzing M3 efficiency, moreover, since the prediction resolution is poor due to the lower granularity of M4, a cluster size of 1 is required on M2 station.

For the analysis of M1 station, based on J/ψ events, the track selection starts from the Ttrack associated to a muon candidate from the J/ψ. Similarly to M2-M5 stations, the robustness of the Ttrack is tested on M2-M5 stations with a 1sigma cut, in X and Y projections, between its extrapolation and the Mtrack cluster. A cut on momentum of 12 GeV/c is applied on the muon candidate and, to improve the purity of the sample, the J/ψ mass is required to lie between $\pm$ 45MeV/c from the PDG value.

7.2 Efficiency measurement procedure

The efficiency for each station is estimated by searching clusters around the prediction defined by a Mtrack reconstructed using the other 4 stations and surviving the described selection. The search is repeated by varying the opening window in a range between 1σ and 8σ in X and Y respectively. The values of σ_x and σ_y are determined, region by region, by a gaussian fit to the central part of the distribution of the distance between the position predicted by the Mtrack in the station under analysis and all clusters in that region. For M1 the prediction is defined by the Ttrack associated to the Mtrack in order to improve its quality. The values of σ_x and σ_y for the twenty regions are reported in table 5.

Obviously the presence of background clusters has an influence on the efficiency determination and in the following sections a detailed description is given on the way the background subtraction is accomplished. The methods to subtract the background for M2-M5 stations and M1 station are described separately in the following sections. The treatment of the background is less critical for M2-M5 stations than for M1 where the occupancy is higher.

[c] A Trigger Sector is a small zone of the detector which is the basic unit where the L0 trigger operates. In most of the cases it is readout by horizontal and vertical strips and the fired zone is identified by crossing the X and Y strips. When there is more than one hit in X and Y the crossing is therefore ambiguous.

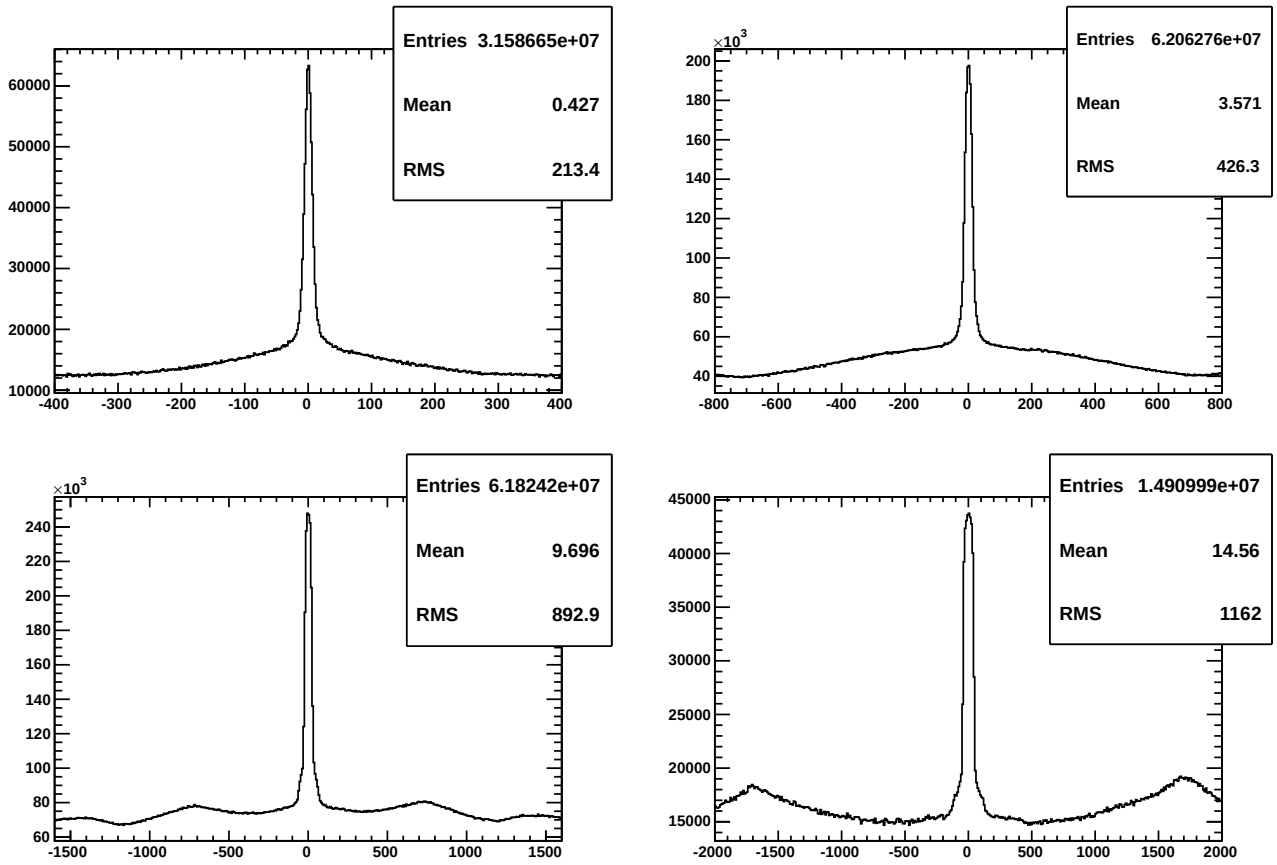

Figure 29 The X difference between all the Ttracks estrapolated in the midplane of M1 station and the M1 clusters. The plots refer to the case in which the M4 station is excluded from the fit, being its efficiency under evaluation. The top left plot are for tracks with extrapolation to R1, the top right to R2, the bottom left to R3 and the bottom right to R4.

In fact on the whole M1 station the average number of clusters in 2010 data is well above 100 while in the downstream stations it ranges from about 20 in M2 to 3 in M5. In the case of M1, therefore, an additional method has been used as a further check of the correctness of the subtraction.

The behaviour of the resulting efficiency as a function of the search opening window will be shown. A correct saturation behaviour for an opening window $> 4\sigma$, both in X and Y, demonstrates that the quality of the track sample is good enough, that the residuals are well described by a gaussian shape and, more importantly, that the background subtraction is a stable and reliable procedure which works even when a search area as large as $16\sigma_x \times 16\sigma_y$ is considered.

7.2.1 Background subtraction for M2-M5 stations

Under the assumption of a poissonian nature of the background, the efficiency can be extracted by fitting the distribution of the cluster multiplicity in the search window. The probability of finding n clusters in the search window is described by the formula

$$P(n) = \epsilon \cdot \frac{B^{n-1} \cdot e^{-B}}{(n-1)!} + (1-\epsilon) \cdot \frac{B^{n} \cdot e^{-B}}{n!} \tag{8}$$

where ϵ is the efficiency and B is the mean value of the background in the search window.

This method to extract the efficiency has the advantage that the background is estimated in the neighboring of the muon track, therefore it takes automatically into account any possible correlation between muons and

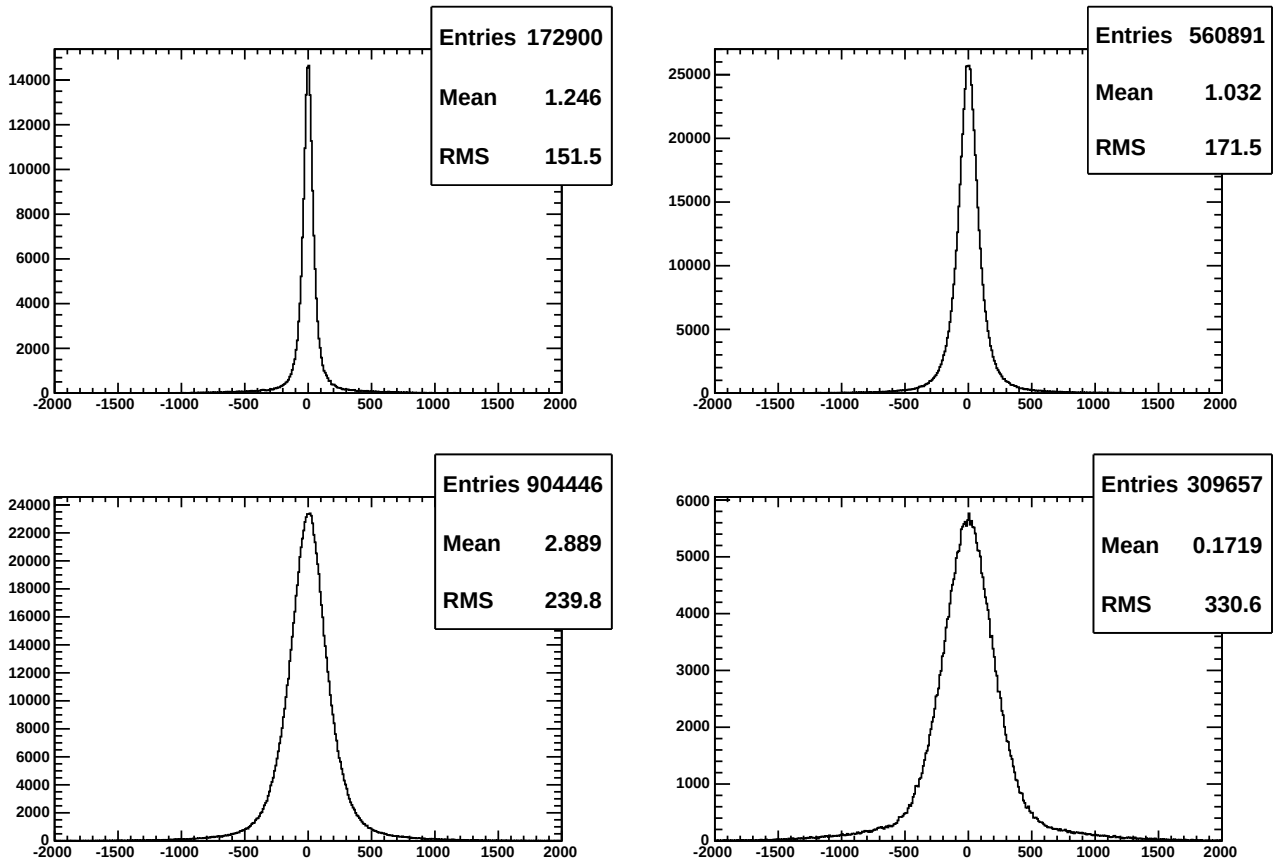

Figure 30 The X difference on the M5 middle plane, between the M5 clusters and the extrapolation of all Ttracks already matched with a Mtrack on M1 station. The plots refer to the case in which the M4 station is excluded from the fit, being its efficiency under evaluation. The top left plot are for tracks with extrapolation to R1, the top right to R2, the bottom left to R3 and the bottom right to R4.

backgrounds as, for instance, in the case of delta rays or punch through in the calorimeter. In figures 33 are reported the fits of the cluster multiplicity distributions of the four regions of stations M3, in the case of an opening window of 8 σ_x and 8 σ_y. The poor quality of the fits, clearly due to the high multiplicity bins, indicates that the model of a simple poissonian background is not sufficiently accurate. A second poissonian component in the fit has been included by modifying the equation 8 as follows:

$$P(n) = \epsilon \cdot [r \cdot \frac{B_1^{n-1} \cdot e^{-B_1}}{(n-1)!} + (1-r) \cdot \frac{B_2^{n-1} \cdot e^{-B_2}}{(n-1)!}] + (1-\epsilon) \cdot [r \cdot \frac{B_1^{n} \cdot e^{-B_1}}{n!} + (1-r) \cdot \frac{B_2^{n} \cdot e^{-B_2}}{n!}] \qquad (9)$$

where B1 and B2 are the two poissonian components of the background and r is their ratio.

In figures 34 are reported the results of the fits with the two background components showing the improvement of the fit quality. However the fitted value of the efficiency does not show any dependence on the chosen background model, demonstrating the reliability of the result.

7.2.2 Background subtraction for M1 station

In fig. 35 are shown, for the J/ψ sample, the M1 cluster multiplicities, within the search window defined in section 3, fitted with the double poissonian function 9. The values of χ^2/N_{dof} indicate that the poissonian background is not a good assumption for M1 as it is for the other stations. Thus another, more direct, method is used on M1

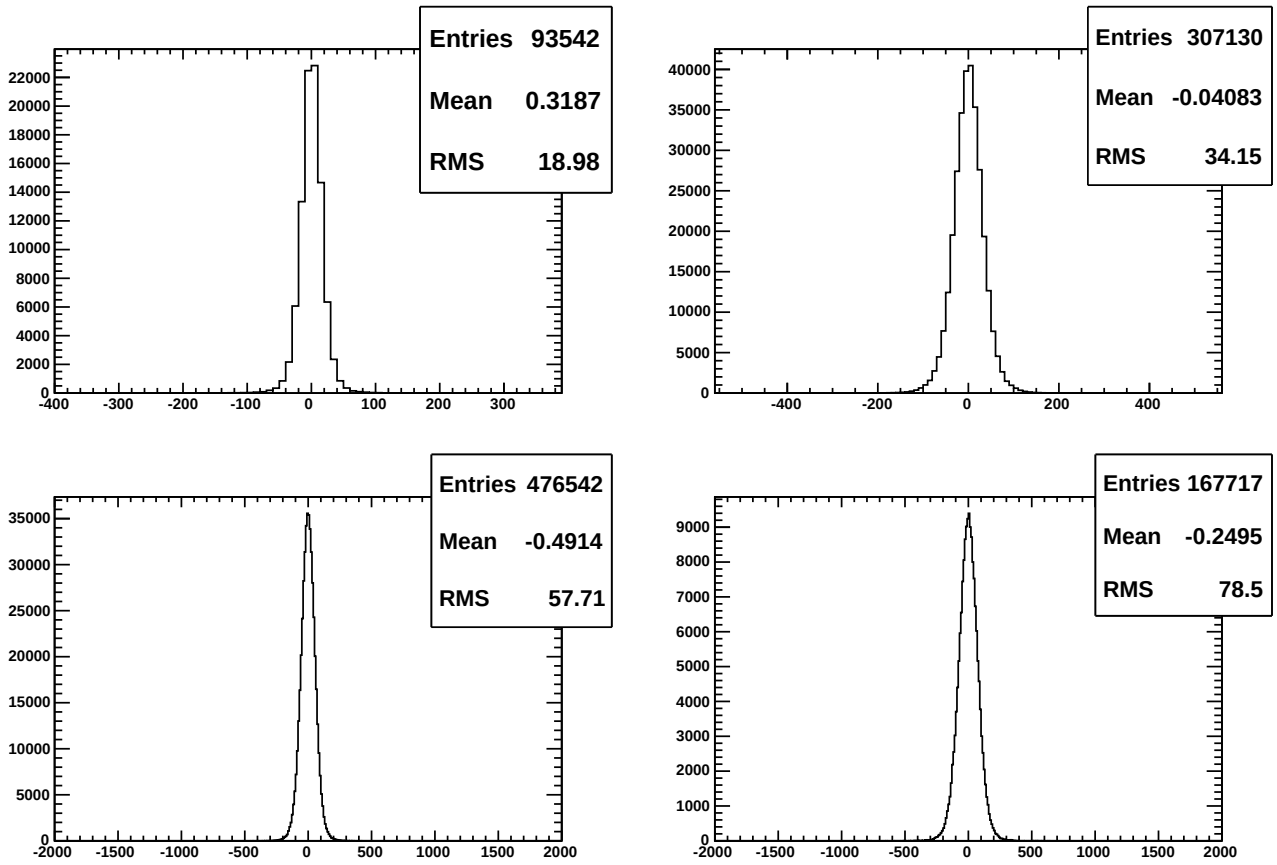

Figure 31 The X difference on the M3 middle plane, between M3 clusters and the extrapolation of all Ttracks already matched with a Mtrack on M1 and M5 stations. The plots refer to the case in which the M4 station is excluded from the fit, being its efficiency under evaluation. The top left plot are for tracks with extrapolation to R1, the top right to R2, the bottom left to R3 and the bottom right to R4.

to evaluate the background. It exploits the ϕ rotation invariance of the primary interactions and assumes that the presence of background correlated with the muon track (for instance delta rays) is negligible. The background is estimated by counting the average number of clusters in the same search window but in the opposite quadrant, with respect to the track prediction. The soundness of the method is confirmed by comparing the number of clusters found in the opposite quadrant with the number of clusters in the track prediction quadrant having subtracted one cluster attributed to the muon track (assumption of 100% efficiency, not too far from reality). as shown for J/ψ events in fig. 36, for the four regions.

The true efficiency ϵ_t is then estimated by the formula:

$$\epsilon_a = \epsilon_t + (1 - \epsilon_t) \cdot P_{bg} \tag{10}$$

where ϵ_a is the apparent efficiency calculated as $N_{NCLUS>0}/N_{Preds}$, being $N_{NCLUS>0}$ the number of tracks where at least one cluster has been found and N_{Preds} the total number of tracks predicted to fall in the search window; $P_{bg} = N^{OQ}_{NCLUS>0}/N_{Preds}$ is the probability to find at least one cluster in the search window in the opposite quadrant.

The efficiency extracted with the two methods described above are in very good agreement as show in the next section.

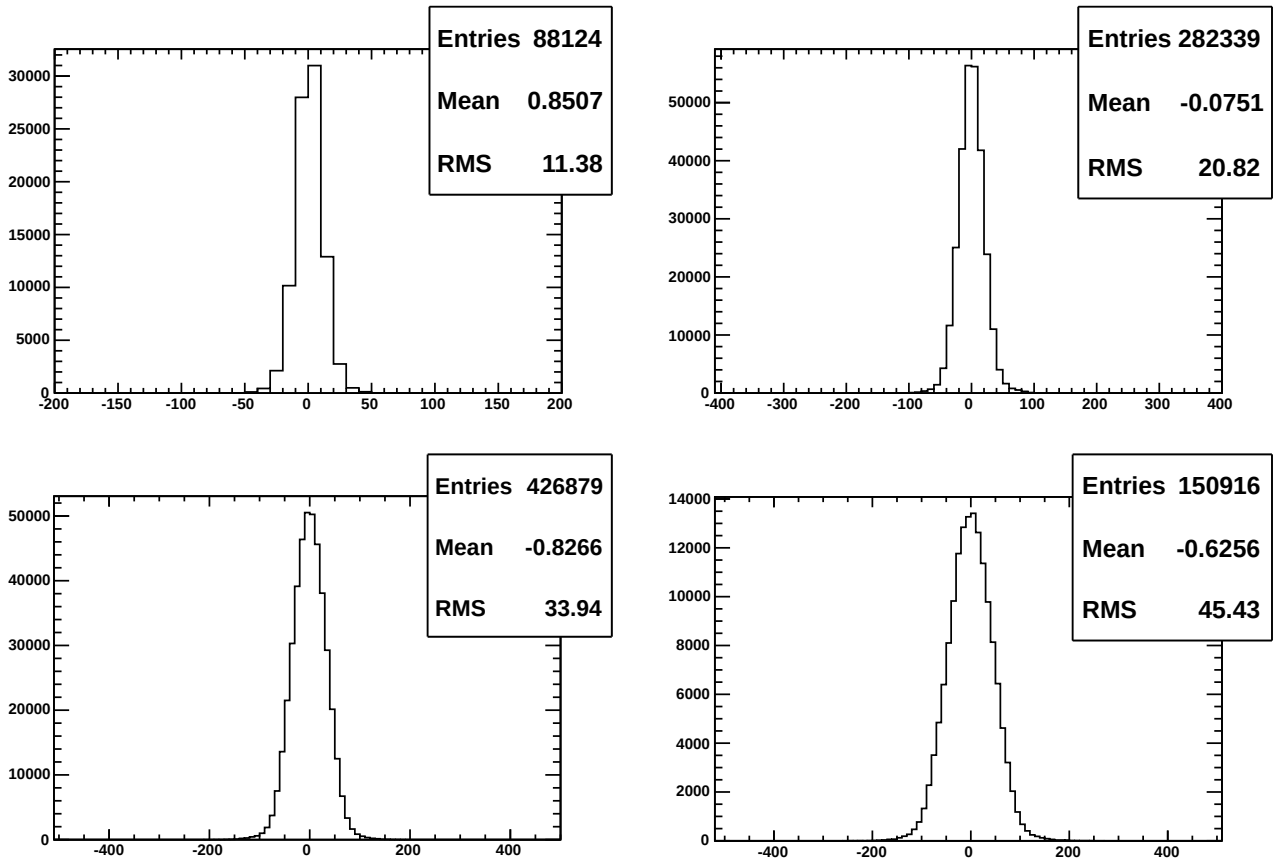

Figure 32 The X difference on the M2 middle plane, between M2 clusters and the extrapolation of all Ttracks already matched with a Mtrack on M1,M3 and M5 stations. The plots refer to the case in which the M4 station is excluded from the fit, being its efficiency under evaluation. The top left plot are for tracks with extrapolation to R1, the top right to R2, the bottom left to R3 and the bottom right to R4.

7.2.3 Check of the procedure

To evaluate that the whole procedure, from track selection to efficiency value determination, is robust and unbiased, a test has been made using simulated events.

As an ideal sample of muon tracks the so-called *Particle Gun* muons have been considered. These muons are generated as starting from the average p-p interaction point with predefined momentum and angular distributions. Since those events are practically background free and do not suffer from fakes in track reconstruction and selection, they allow to cleanly extract the efficiency measurable with the present method. The absolute value depends on the assumptions made in the digitization procedure and on geometrical effects and will not be necessarily in agreement with the value obtained with real data. The efficiency obtained on *Particle Gun* events is then compared with the one obtained on Minimum Bias (MB), for M2-M5, and J/ψ, for M1, MC events where all background components and detector effects are supposed to be well reproduced. A satisfactory comparison is an overall check of the correctness of the procedure, in particular of the background subtraction method.

The estimated values for the different stations and regions are reported in table 6. The agreement is good apart from R3 and R4 regions of the M5 station where the efficiency extracted from the Minimum bias is lower than the corresponding *Particle Gun* efficiency. This difference is due to the track selection purity. In fact part of the reconstructed tracks, surviving to the cleaning cuts, are muons produced inside the calorimeter shower that are aligned with the hadron track initiating the shower. These muons have an unknown momentum. In case of low muons, the track can be absorbed between M4 and M5 causing artificial inefficiency in M5. This effect is region dependent since, on average, track crossing the outers region have on average lower momentum that those traversing inner regions. In fact, in the Minimum Bias Monte Carlo events the fraction of selected tracks having the muon with momentum lower than the minimum value required to reach M5 (6 GeV/c) is 0.2% in R1, 0.3% in R2, 0.7%

Table 5 Resolution along X and Y of the distance between the muon track and the muon cluster in each region of the muon detector. The muon track is reconstructed skipping the station of which the resolution must be evaluated. For M1 station the numbers refer to the J/ψ sample.

		$\sigma_x(mm)$	$\sigma_y(mm)$
	M1R1	4	10
	M1R2	8	18
	M1R3	16	40
	M1R4	32	80
	M2R1	15	30
	M2R2	25	50
	M2R3	35	70
	M2R4	60	100
	M3R1	10.	12.
	M3R2	15.	24.
	M3R3	25.	48.
	M3R4	40.	96.
	M4R1	15.	16.
	M4R2	27.	32.
	M4R3	48.	64.
	M4R4	97.	128.
	M5R1	33	40
	M5R2	50	60
	M5R3	100	110
	M5R4	150	180

in R3 and 1.5% in R4. Removing the tracks with momentum below 6 GeV/c, the efficiency reaches the value of 99.77 ± 0.07 in R1, 99.63 ± 0.04 in R2, 99.51 ± 0.08 in R3 and 99.8 ± 0.1 in R4 in the minimum bias sample, in agreement with the *Particle Gun*. To take into account such effect the real data results have been corrected for the ratio between the efficiencies with and without the 6 GeV/c cut, as extracted by the Minimum Bias Monte Carlo sample.

Table 6 Values of the MonteCarlo efficiency for Minimum Bias and $J\psi$ events compared to *Particle Gun* Monte-Carlo events.

		R1	R2	R3	R4
M1	PG	95. $\pm$ 1.	94.9 $\pm$ 0.4	95.0 $\pm$ 0.2	97.6 $\pm$ 0.2
	J/ψ	93.5 $\pm$ 0.2	94.4 $\pm$ 0.1	94.7 $\pm$ 0.2	97.3 $\pm$ 0.4
M2	PG	99.5 $\pm$ 0.2	99.67 $\pm$ 0.09	99.70 $\pm$ 0.05	99.96 $\pm$ 0.03
	MB	99.56 $\pm$ 0.07	99.69 $\pm$ 0.04	99.61 $\pm$ 0.08	100 $\pm$ 7
M3	PG	99.9 $\pm$ 0.4	99.73 $\pm$ 0.07	99.68 $\pm$ 0.05	99.92 $\pm$ 0.02
	MB	99.64 $\pm$ 0.07	99.59 $\pm$ 0.05	99.70 $\pm$ 0.08	99.87 $\pm$ 0.1
M4	PG	99.9 $\pm$ 0.2	99.61 $\pm$ 0.09	99.70 $\pm$ 0.05	99.94 $\pm$ 0.03
	MB	99.58 $\pm$ 0.05	99.64 $\pm$ 0.03	99.65 $\pm$ 0.07	99.84 $\pm$ 0.1
M5	PG	99.5 $\pm$ 0.3	99.73 $\pm$ 0.09	99.69 $\pm$ 0.06	99.88 $\pm$ 0.03
	MB	99.58 $\pm$ 0.07	99.46 $\pm$ 0.04	99.14 $\pm$ 0.07	99.0 $\pm$ 0.2
	MB (P$>$ 6 GeV/c)	99.77 $\pm$ 0.07	99.63 $\pm$ 0.04	99.51 $\pm$ 0.08	99.8 $\pm$ 0.1

7.3 Results

In the following the behaviour of the efficiency as a function of the number of σ's of the opening window will be shown for all regions of the muon system. The attainment of the saturation at 4-5 $sigma$ shows the reliability of the method. However the final value of the efficiency evaluated with the present analysis will be the one at 8 σ to allow for the presence of non gaussian tails in the prediction point.

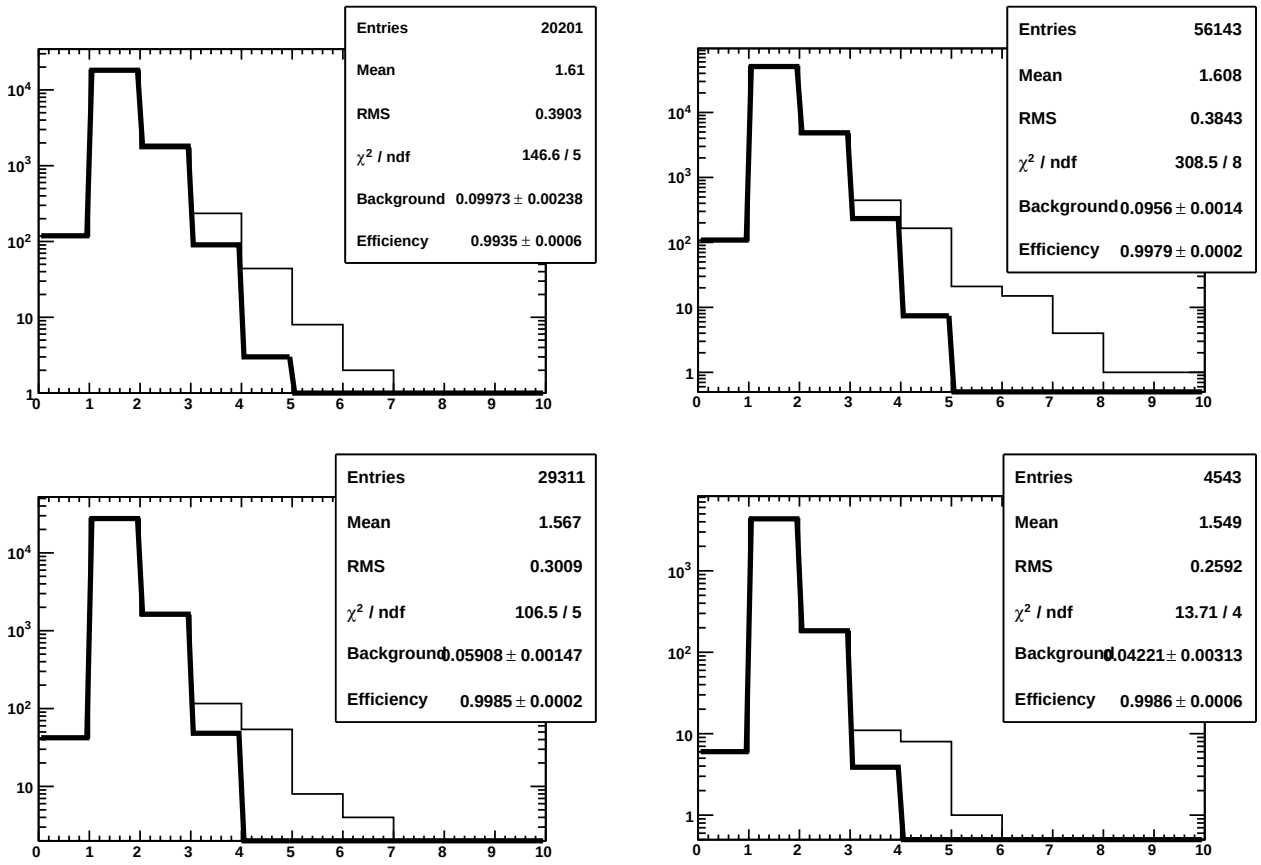

Figure 33 The cluster multiplicity in search windows in the four M3 regions. The thick line corresponds to the fit done with the single background component described in equation 8.

7.3.1 Stations M2-M5

The behaviour of the efficiency as a function of the number of σ for the four regions of M2, M3, M4 and M5 are shown in figures 37, 38, 39 and 40 respectively.

The summary of the results for M2,M3,M4 and M5 stations are reported in table 7, 8,9 and 10 respectively, where the values of the efficiency at 4 σ and at 8 σ are shown.

Two specific small zones in M3R2 and M4R2 were excluded due to the pathologies mentioned on section 2.2, corresponding to, approximately, a loss of 1.8% and 0.3% respectively for the efficiency of such regions.

For all stations a small loss of about 0.1% was also recovered excluding a central band of $\pm$ 3 σ_x along the X direction to take into account the separation region between the two half-stations.

7.3.2 M1 station

The efficiencies obtained with equation 10 are shown in fig 41. In table 11 the numerical values are reported. In the same table the value of the efficiency obtained with the double gaussian fit to the cluster multiplicity distribution is also reported, showing that the agreement is excellent. The final value of the efficiency is the average of the two estimates. To obtain the efficiencies in table 11 a series of geometrical cuts had to be applied. As mentioned on section 2.2, three chambers were known to be highly inefficient due to hardware problems, namely A22C and A24C in region 4, and A16A2 in region 1. They were excluded from the analysis recovering an efficiency loss of 1.2% and 5.5% in region 4 and region 1 respectively. In addition two small zones in regions 2 and 3 with efficiency losses of about 0.1% were discarded. A small area along the junction of side A and C was also excluded to get rid of the corresponding geometrical loss of about 0.1%.

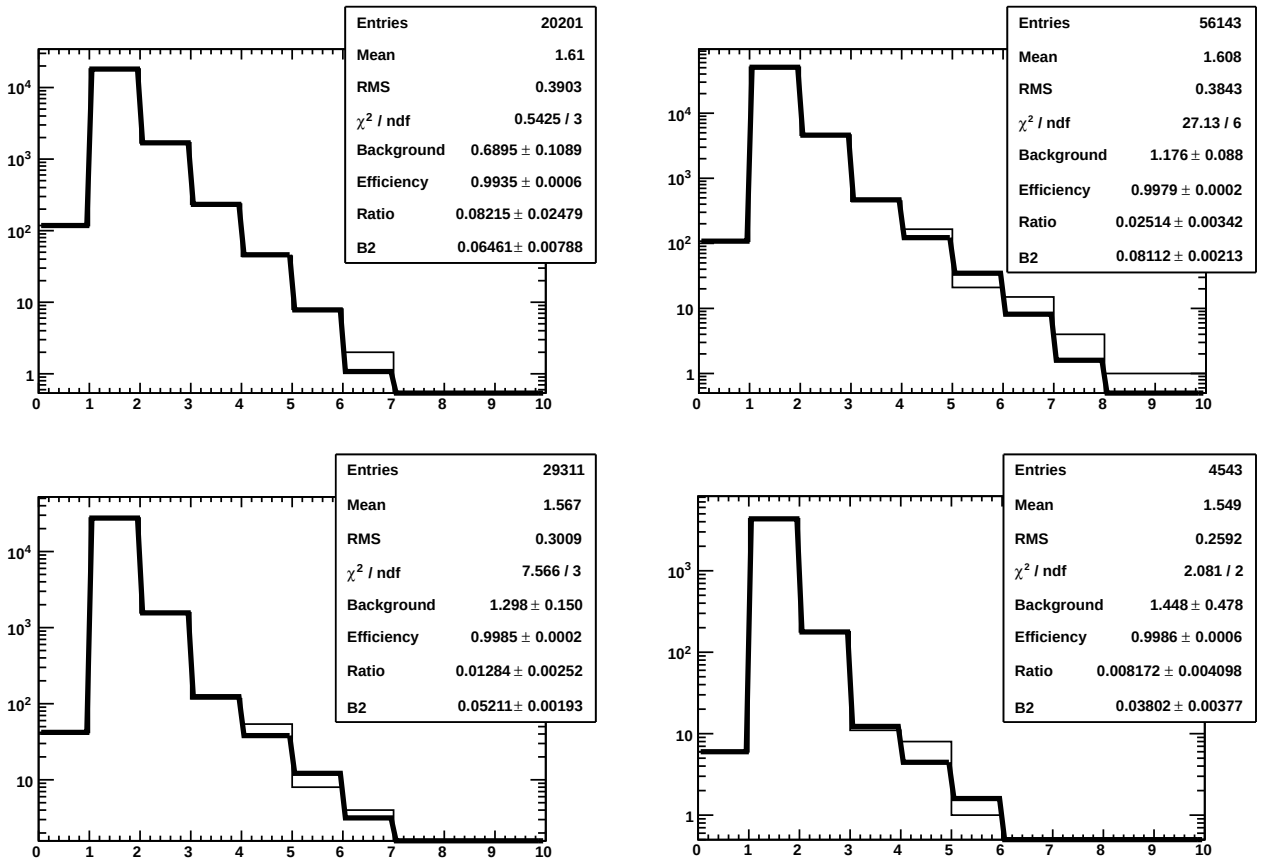

Figure 34 The cluster multiplicity in search windows in the four M3 regions. The thick line shows the results of the fit with two background components described in equation 9.

7.3.3 Systematic uncertainties

For M2-M5 the systematic error due to background modeling has been estimated by changing the fit function from two poissonians to a single one. The efficiency varies less that 0.01% in all regions of M2-M5.

For M1 two orthogonal ways of estimating the background have been adopted, i.e. with the double poissonian background fit as in M2-M5 and by measuring the background in the opposite quadrant. A systematic uncertainty of half the difference between the two, has been assumed.

Since the choice of evaluating the final efficiency at 8σ has a certain degree of arbitrariness, a systematic error has been assigned as half the difference between the efficiency value calculated at $4\ \sigma$ and $8\ \sigma$, both in X and Y projections.

The uncertainty, due to MC limited statistics, of the correction applied on the M5 efficiency to take into account the absorption of muons between M4 and M5 is included in the systematics.

In table 12 is reported the final summary of the efficiencies with the statistical and systematic errors for all the twenty regions of the muon detector. The different systematic sources have been added in quadrature.

7.4 Comparison with timing efficiency

Our final estimates of the total efficiency of each region are compared in figure 42 with the results of section 6.2 where the contribution of timing tails to the inefficiency is evaluated. As already mentioned, the limited statistics of TAE data prevented to apply the same track selection for the two studies. The lower purity of the muon track sample for the timing analysis leads to an underestimation of the timing efficiency. The data were also acquired at different times, and this could explain the poorer performances of region M1R1 for the TAE acquired at the end

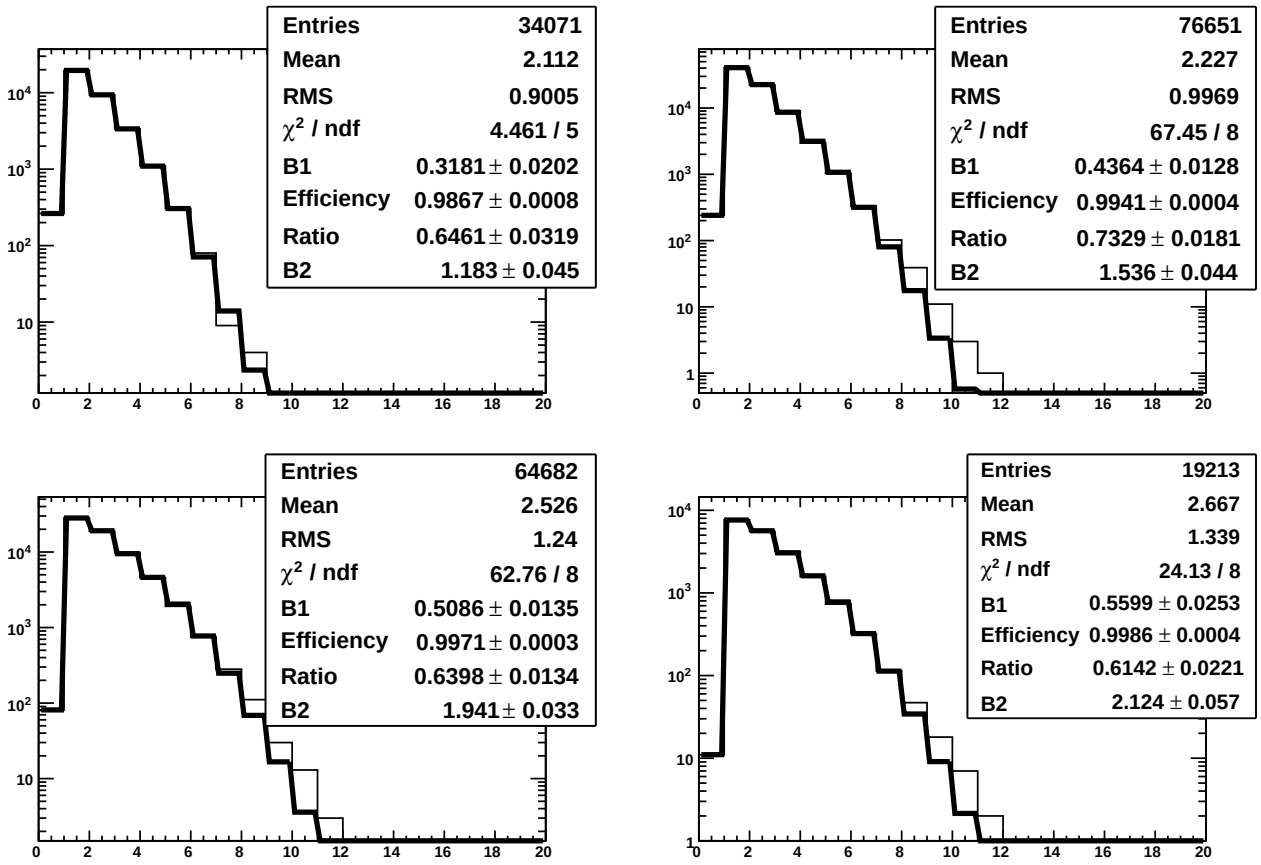

Figure 35 The cluster multiplicity within 8 σ search window for the four M1 regions is shown for J/ψ events. The fit with the assumption of a double poissonian background is superimposed

of the runs with a slightly lower high voltage (see section 2.2). Nevertheless, the region dependence of the two measurements is very similar, and for the regions less affected by combinatorial background the timing efficiency is found to be compatible or slightly better than the total efficiency, suggesting that the bulk of inefficiency comes from signals falling outside the 25ns LHC gate.

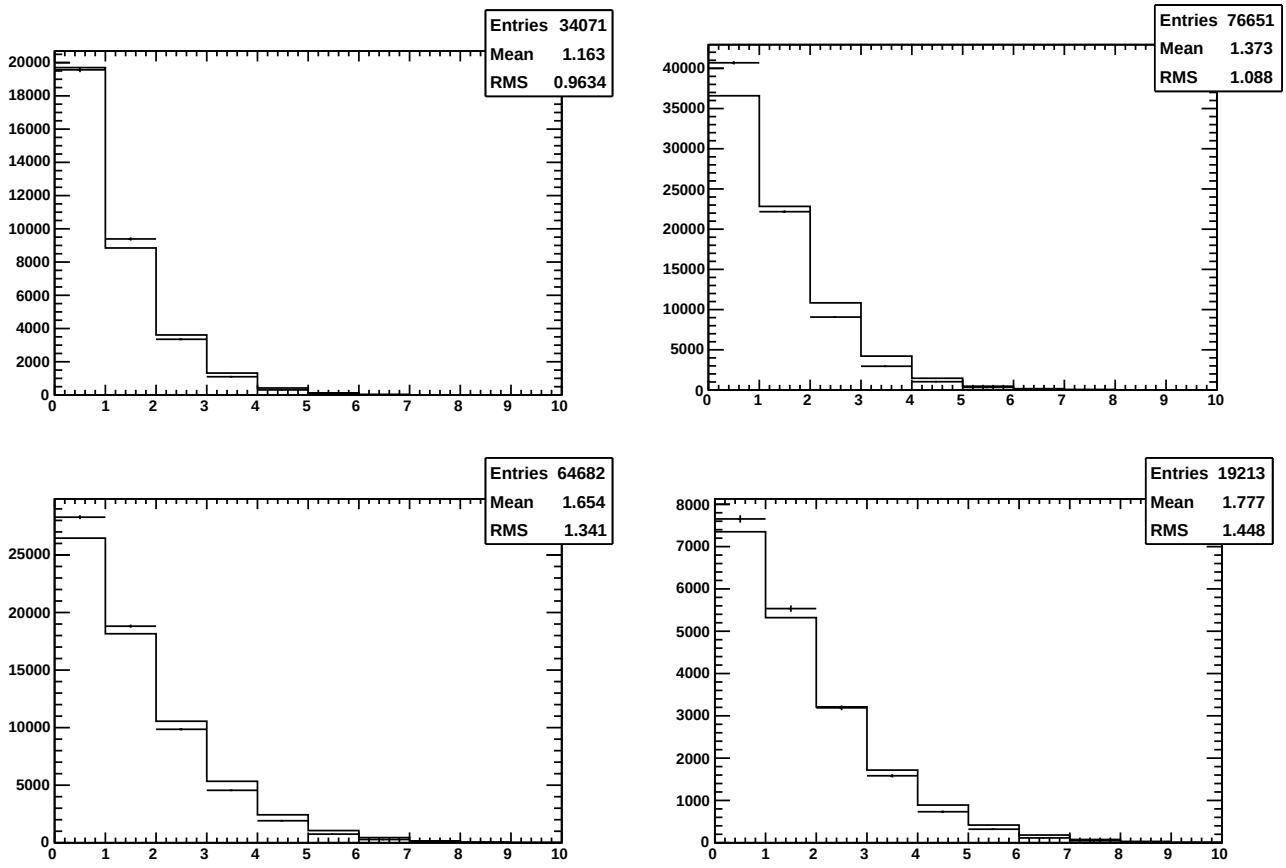

Figure 36 The cluster multiplicity in the prediction quadrant diminished by 1 (histogram) and the cluster multiplicity in the same search window but in the opposite quadrant (dots), shown for the four regions of M1 station for J/ψ events.

Table 7 M2 station: number of tracks reconstructed in each region for MB data, fit results at 8σ search window, and value of the efficiency at 4σ search window.

M2R1	Tracks	14898
	Efficiency	99.68 ± 0.05
	χ^2/dof	0.8/2
	Efficiency (4σ)	99.61 ± 0.05
M2R2	Tracks	29074
	Efficiency	99.78 ± 0.03
	χ^2/dof	31.5/4
	Efficiency (4σ)	99.69 ± 0.03
M2R3	Tracks	13649
	Efficiency	99.79 ± 0.04
	χ^2/dof	41.1/3
	Efficiency (4σ)	99.75 ± 0.04
M2R4	Tracks	1345
	Efficiency	99.8 ± 0.1
	χ^2/dof	3.2/1
	Efficiency (4σ)	99.8 ± 0.1

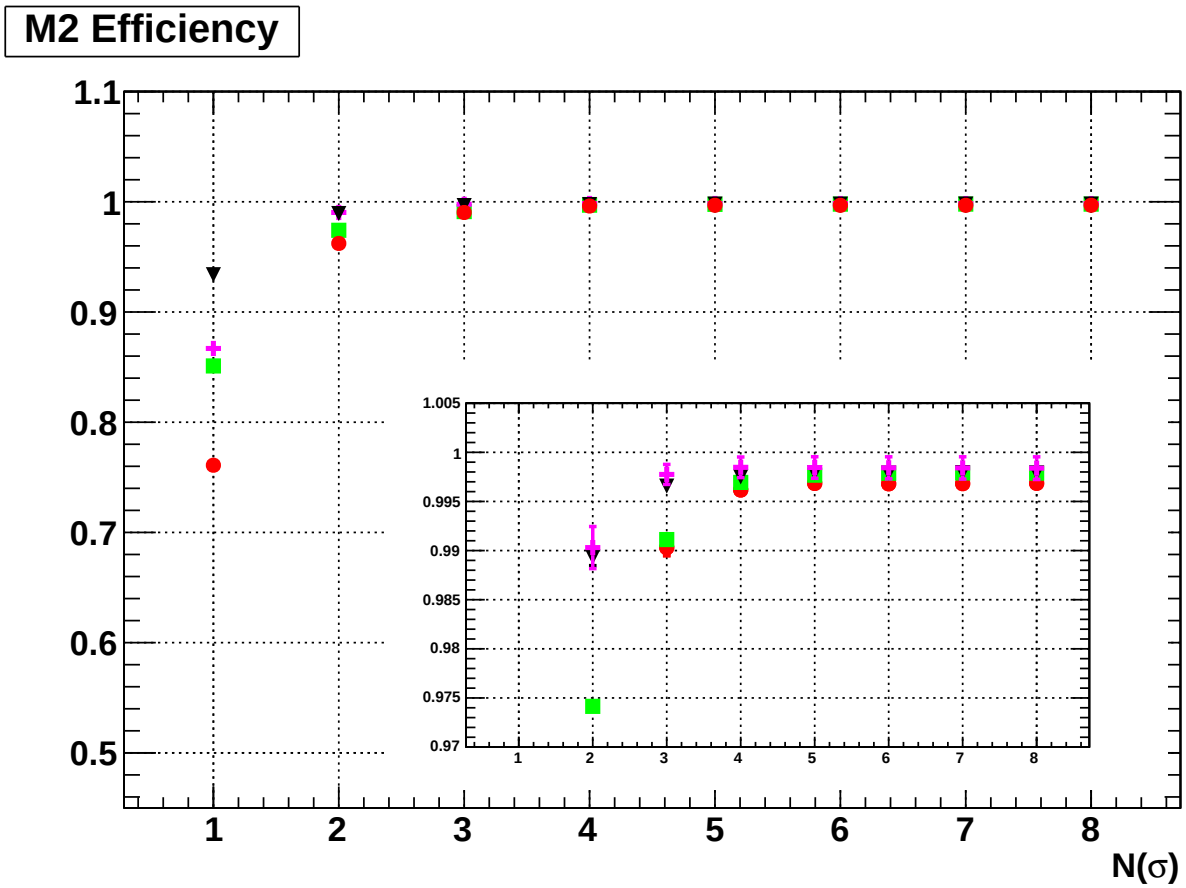

Figure 37 The measured efficiency of M2 station as a function of the number of σ in the search window. The four regions are shown: R1 (red circles), R2(green squares), R3(black triangles), R4(pink crosses)

Table 8 M3 station: number of tracks reconstructed in each region for MB data, fit results at 8σ search window, and value of the efficiency at 4σ search window.

M3R1	Tracks	20201
	Efficiency	99.35 ± 0.06
	χ^2/dof	0.5/3
	Efficiency (4σ)	99.25 ± 0.06
M3R2	Tracks	56143
	Efficiency	99.79 ± 0.02
	χ^2/dof	27.1/6
	Efficiency (4σ)	99.71 ± 0.02
M3R3	Tracks	29311
	Efficiency	99.85 ± 0.02
	χ^2/dof	7.6/3
	Efficiency (4σ)	99.83 ± 0.02
M3R4	Tracks	4543
	Efficiency	99.86 ± 0.06
	χ^2/dof	2.1/2
	Efficiency (4σ)	99.86 ± 0.05

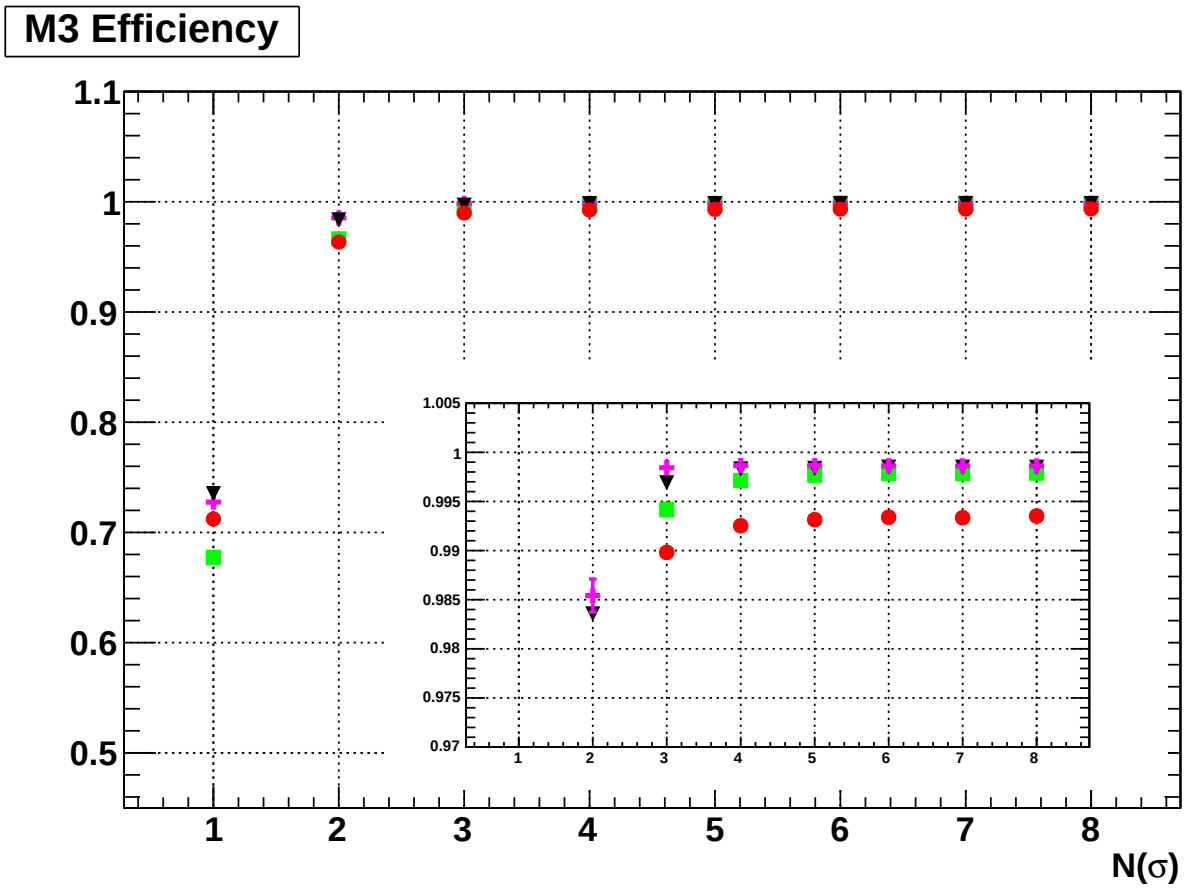

Figure 38 The measured efficiency of M3 station as a function of the number of σ in the search window. The four regions are shown: R1 (red circles), R2(green squares), R3(black triangles), R4(pink crosses)

Table 9 M4 station: number of tracks reconstructed in each region for MB data, fit results at 8σ search window, and value of the efficiency at 4σ search window.

M4R1	Tracks	42651
	Efficiency	99.62 ± 0.03
	χ^2/dof	1.4/3
	Efficiency (4σ)	99.49 ± 0.03
M4R2	Tracks	80220
	Efficiency	99.89 ± 0.01
	χ^2/dof	2.4/3
	Efficiency (4σ)	99.83 ± 0.01
M4R3	Tracks	21478
	Efficiency	99.65 ± 0.04
	χ^2/dof	18.5/2
	Efficiency (4σ)	99.59 ± 0.04
M4R4	Tracks	3352
	Efficiency	99.72 ± 0.09
	χ^2/dof	8.4/2
	Efficiency (4σ)	99.73 ± 0.09

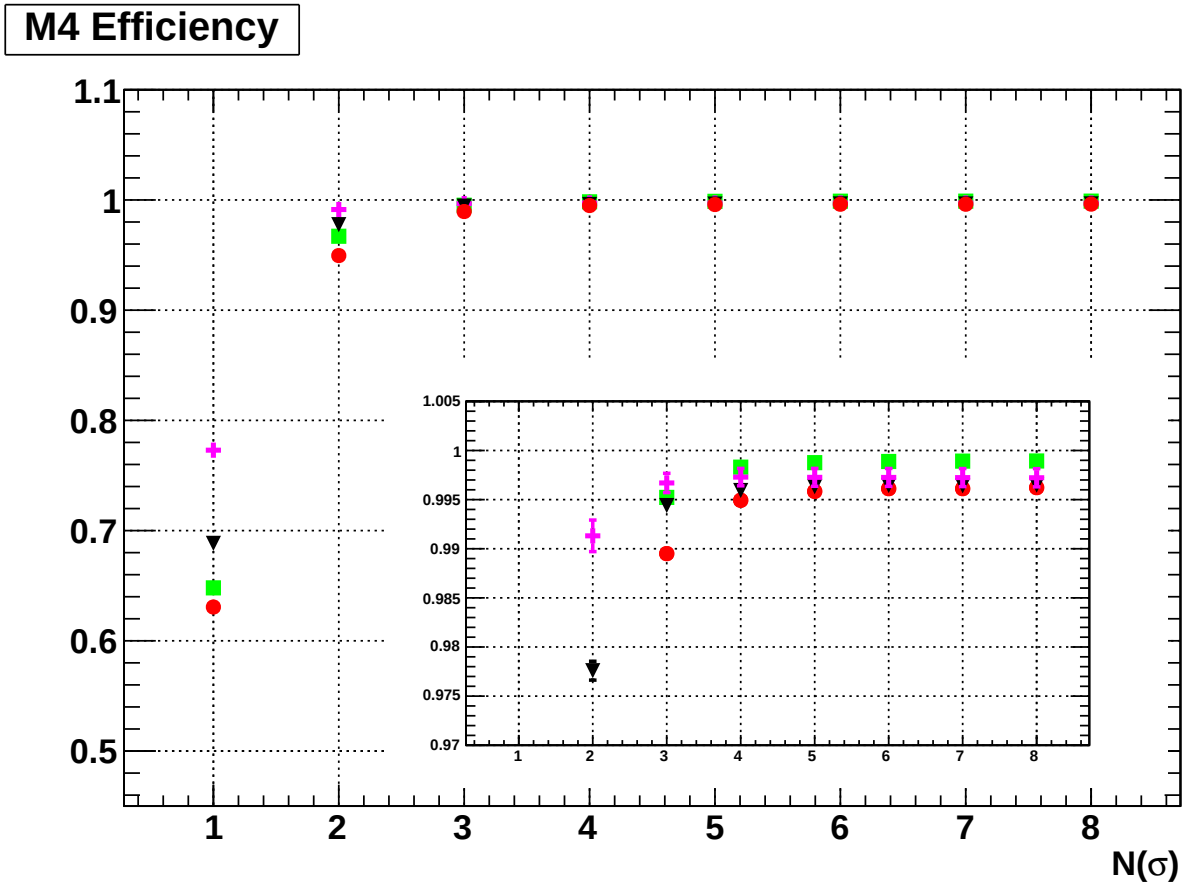

Figure 39 The measured efficiency of M4 station as a function of the number of σ in the search window. The four regions are shown: R1 (red circles), R2(green squares), R3(black triangles), R4(pink crosses)

Table 10 M5 station: number of tracks reconstructed in each region for MB data, fit results at 8σ search window, and value of the efficiency at 4σ search window. The value of the efficiency corrected for the absorption between station M4 and M5 is reported also (see 7.2.3 section).

M5R1	Tracks	12207
	Efficiency	99.45 ± 0.07
	χ^2/dof	1.2/4
	Efficiency (4σ)	99.45 ± 0.07
	Corrected efficiency	99.6 ± 0.1
M5R2	Tracks	42532
	Efficiency	99.63 ± 0.03
	χ^2/dof	0.1/1
	Efficiency (4σ)	99.59 ± 0.03
	Corrected efficiency	99.82 ± 0.06
M5R3	Tracks	21338
	Efficiency	99.61 ± 0.04
	χ^2/dof	23.6/2
	Efficiency (4σ)	99.58 ± 0.04
	Corrected efficiency	100.0 ± 0.1
M5R4	Tracks	2649
	Efficiency	99.2 ± 0.2
	χ^2/dof	0/0
	Efficiency (4σ)	99.2 ± 0.2
	Corrected efficiency	100.0 ± 0.2

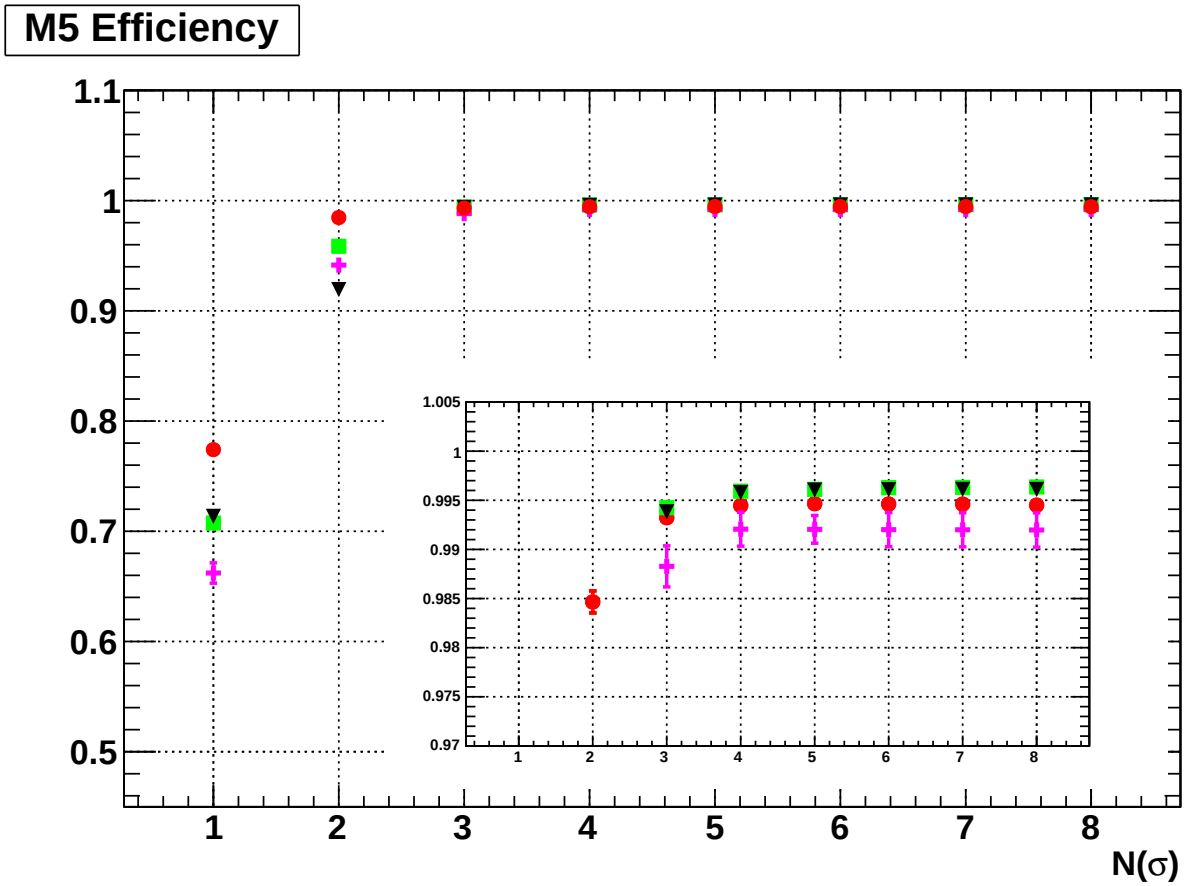

Figure 40 The measured efficiency of M5 station as a function of the number of σ in the search window. The four regions are shown: R1 (red circles), R2(green squares), R3(black triangles), R4(pink crosses)

Table 11 M1 station: number of tracks reconstructed in each region for J/ψ data, fit results at 8σ search window, and value of the efficiency at 4σ search window. For each region the resulting efficiency obtained by fitting the cluster multiplicity distribution with a double poissonian assumption for the background (eq 8) is also shown.

M1R1	Tracks	14632
	Efficiency	98.66 ± 0.08
	Efficiency (4σ)	98.50 ± 0.07
	Efficiency eq.8	98.67 ± 0.08
M1R2	Tracks	50422
	Efficiency	99.34 ± 0.04
	Efficiency (4σ)	99.21 ± 0.04
	Efficiency eq.8	99.41 ± 0.04
M1R3	Tracks	35282
	Efficiency	99.69 ± 0.03
	Efficiency (4σ)	99.58 ± 0.03
	Efficiency eq.8	99.71 ± 0.03
M1R4	Tracks	10153
	Efficiency	99.85 ± 0.04
	Efficiency (4σ)	99.82 ± 0.03
	Efficiency eq.8	98.86 ± 0.04

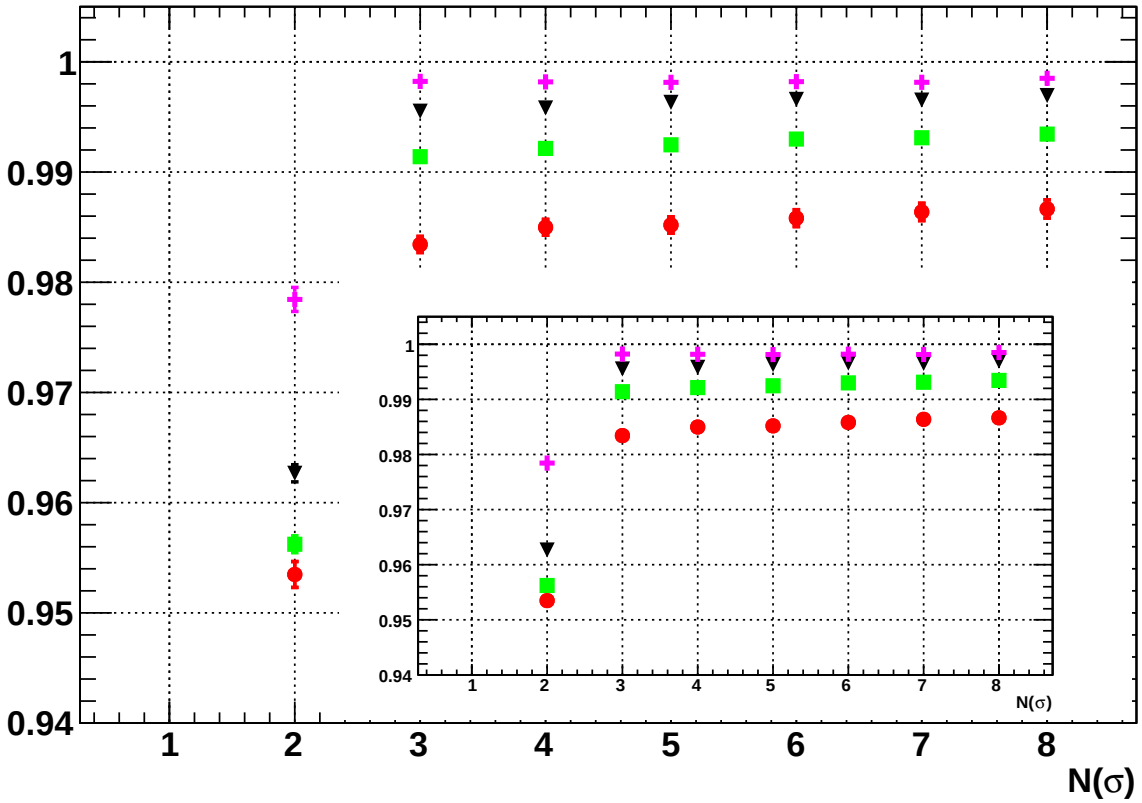

Figure 41 The measured efficiency of M1 station as a function of the number of σ in the search window. The four regions are shown: R1 (red circles), R2(green squares), R3(black triangles), R4(pink crosses)

Table 12 Efficiency values of all the twenty regions with their statistical and systematic errors

	R1	R2	R3	R4
M1	$98.66 \pm 0.08 \pm 0.08$	$99.37 \pm 0.04 \pm 0.08$	$99.70 \pm 0.03 \pm 0.06$	$99.85 \pm 0.04 \pm 0.02$
M2	$99.68 \pm 0.05 \pm 0.04$	$99.78 \pm 0.03 \pm 0.05$	$99.79 \pm 0.04 \pm 0.02$	$99.8 \pm 0.1 \pm 0.01$
M3	$99.35 \pm 0.06 \pm 0.05$	$99.79 \pm 0.02 \pm 0.04$	$99.85 \pm 0.02 \pm 0.01$	$99.86 \pm 0.06 \pm 0.01$
M4	$99.62 \pm 0.03 \pm 0.07$	$99.89 \pm 0.01 \pm 0.03$	$99.65 \pm 0.04 \pm 0.03$	$99.72 \pm 0.09 \pm 0.01$
M5	$99.64 \pm 0.07 \pm 0.10$	$99.82 \pm 0.03 \pm 0.04$	$99.90 \pm 0.04 \pm 0.12$	$100.0 \pm 0.2 \pm 0.1$

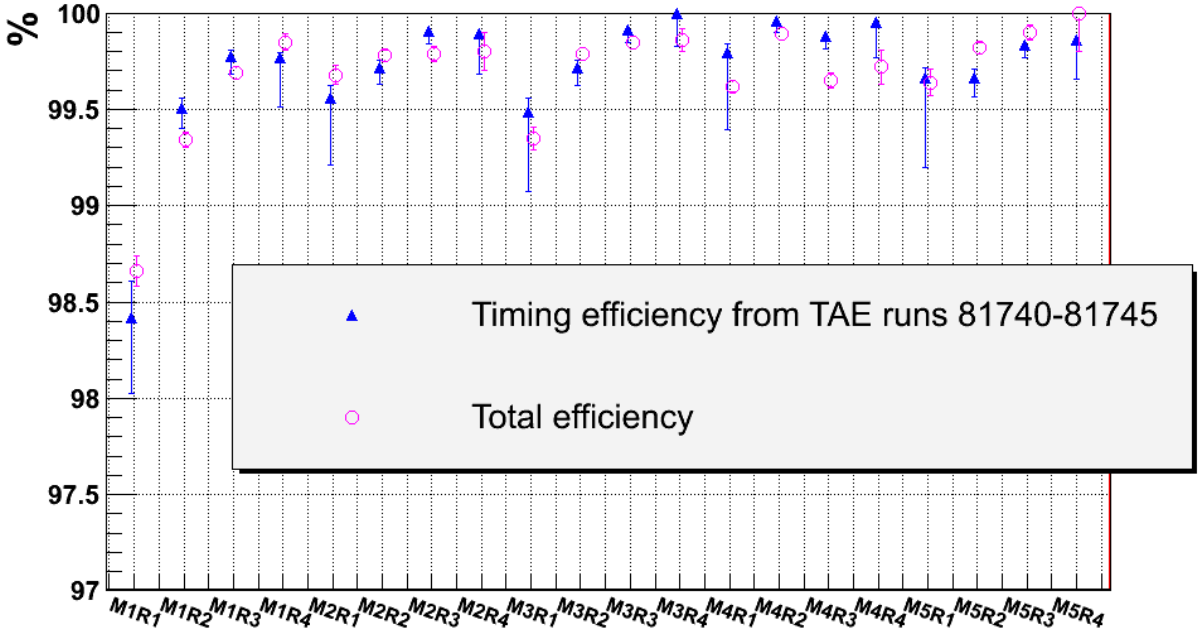

Figure 42 The results for total efficiency are compared with the estimates of timing efficiency from section 6.2. Errors are statistical only. For the regions most affected by combinatorial background (M1, M5, region 1) a systematic underestimation of the timing efficiency by a few per mill is probably present.

8 Conclusions

The muon detector was successfully operated during the first year of LHC physics. Detector performance was carefully evaluated in this note, showing that all the requirements have been fullfilled. Notably, the whole detector chain demonstrated an excellent reliability and stability among the five orders of magnitude of luminosity experienced during 2010, with maximum particle rates comparable to the design values. A careful timing intercalibration allowed to reach the required time resolution of 3 ns for the whole detector, except for the slightly worse performances in region M1R1 where GEM chambers were operated with higher than expected particle rates. The efficiency has been evaluated in each region of the muon detector after having excluded from the analysis small regions with evident instrumental problems. The obtained value has to be intended as an average over the region. Apart from an expected slightly lower value in M1R1, the resulting efficiencies are all well above the design requirement of 99% value within errors.

9 Aknowledgments

We would like to thank Giuseppe Martellotti for his constructive criticisms and for the very careful reading of this document.

10 References

[1] Muon System TDR The LHCb collaboration LHCC 2001-010

[2] M. Anelli *et al.*, "Performance of the LHCb muon system with cosmic rays," JINST **5** (2010) P10003.

[3] A. Kashchuk and O.V. Levitskaya, "From Noise to Signal – a new approach to LHCB muon optimization", CERN-LHCb-PUB-2009-018, Jan 2010

[4] A. Kashchuk, R. Nobrega and A. Sarti, "Procedure for determination and setting of thresholds implemented in the LHCb Muon system", CERN-LHCb-2008-052, Oct 2008

[5] E. Aslanides et al., "Performance of the muon trigger with a realistic simulation", CERN-LHCb-2002-041 (2002)

[6] G. Martellotti, R. Santacesaria, A. Satta, "Particle rates in the LHCb muon detector", CERN-LHCb-2005-075 (2005)

[7] W. Bonivento *et al*, "Measurement of the time resolution of the installed muon chambers with the 2008 cosmic runs", CERN-LHCb-PUB-2009-016 (2009)

[8] E. Dane, A. Sarti, G. Penso, D. Pinci, "Detailed study of the gain of the MWPCs for the LHCb muon system," Nucl. Instrum. Meth. **A572** (2007) 682-688.

[9] Studies of Efficiency of the LHCb Muon Detector Using Cosmic Rays Manca G. Mou L. Saitta B. CERN-LHCb-PUB-2009-017

[10] Muon identification in the LHCb High Level Trigger Satta A. CERN-LHCb-2005-071.

[11] T. Sostrand, S. Mrenna and P.Z. Skands, "PYTHIA 6.4 physics and manual", version 6.422, J. High Energy Phys. 0605 (2006) 026.

[12] S. Agostinelli et al. [GEANT4 Collaboration], "GEANT4: a simulation toolkit", version 9.2, Nucl. Instrum. Meth. A 506 (2003) 250.